Biophysical *Journal*
Article

Biophysical Society

Dynamics of the *E. coli* β-Clamp Dimer Interface and Its Influence on DNA Loading

Bilyana N. Koleva,[1] Hatice Gokcan,[2] Alessandro A. Rizzo,[3] Socheata Lim,[3] Kevin Jeanne Dit Fouque,[4] Angelina Choy,[1] Melissa L. Liriano,[1] Francisco Fernandez-Lima,[4] Dmitry M. Korzhnev,[3] G. Andrés Cisneros,[2] and Penny J. Beuning[1,*]

[1]Department of Chemistry and Chemical Biology, Northeastern University, Boston, Massachusetts; [2]Department of Chemistry, University of North Texas, Denton, Texas; [3]Department of Molecular Biology and Biophysics, University of Connecticut Health Center, Farmington, Connecticut; and [4]Department of Chemistry and Biochemistry, Florida International University, Miami, Florida

ABSTRACT The ring-shaped sliding clamp proteins have crucial roles in the regulation of DNA replication, recombination, and repair in all organisms. We previously showed that the *Escherichia coli* β-clamp is dynamic in solution, transiently visiting conformational states in which Domain 1 at the dimer interface is more flexible and prone to unfolding. This work aims to understand how the stability of the dimer interface influences clamp-opening dynamics and clamp loading by designing and characterizing stabilizing and destabilizing mutations in the clamp. The variants with stabilizing mutations conferred similar or increased thermostability and had similar quaternary structure as compared to the wild type. These variants stimulated the ATPase function of the clamp loader, complemented cell growth of a temperature-sensitive strain, and were successfully loaded onto a DNA substrate. The L82D and L82E I272A variants with purported destabilizing mutations had decreased thermostability, did not complement the growth of a temperature-sensitive strain, and had weakened dimerization as determined by native trapped ion mobility spectrometry-mass spectrometry. The β L82E variant had a reduced melting temperature but dimerized and complemented growth of a temperature-sensitive strain. All three clamps with destabilizing mutations had perturbed loading on DNA. Molecular dynamics simulations indicate altered hydrogen-bonding patterns at the dimer interface, and cross-correlation analysis showed the largest perturbations in the destabilized variants, consistent with the observed change in the conformations and functions of these clamps.

SIGNIFICANCE The relationship between protein dynamics and function is still poorly understood. The bacterial β sliding clamp displays dynamic behavior at the dimer interface, raising the possibility that the clamp is transiently open. To test the role of dynamics in clamp function, we designed stabilizing and destabilizing mutations at and near the dimer interface. Clamp variants with destabilized dimer interfaces generally had altered thermal stability and dimerization and did not support bacterial growth. Molecular dynamics simulations support the model of interface perturbation because the variants with destabilizing mutations have dramatically altered hydrogen-bonding patterns at the dimer interface.

INTRODUCTION

The ring-shaped sliding processivity clamp protein of the DNA replication machinery has crucial roles in the regulation of DNA replication, recombination, and repair in all living organisms and some viruses. DNA polymerases replicate the genomes of entire organisms, and the sliding processivity clamp provides the speed and processivity required by DNA polymerases for efficient DNA replication (1–3). The sliding clamp binds the polymerase and tethers it to DNA, allowing the polymerase to replicate DNA without dissociation from the template. Structural studies reveal that sliding clamps have a pseudo-sixfold symmetry and individual subunits are arranged in a head-to-tail conformation (1,4–8). Clamps from bacterial species (4) are homodimeric, with three domains in each monomer, whereas eukaryotic and archaeal species (5,9–11) are trimers with two domains in each monomer. Each domain consists of two α-helices and two four-stranded antiparallel β-sheets; adjacent α-helices and a long curved β-sheet provide the interdomain interactions (Fig. 1). The *Escherichia coli* β-clamp increases the processivity and speed of replication

Submitted February 1, 2019, and accepted for publication June 27, 2019.

*Correspondence: beuning@neu.edu

Editor: Elizabeth Komives.

https://doi.org/10.1016/j.bpj.2019.06.035

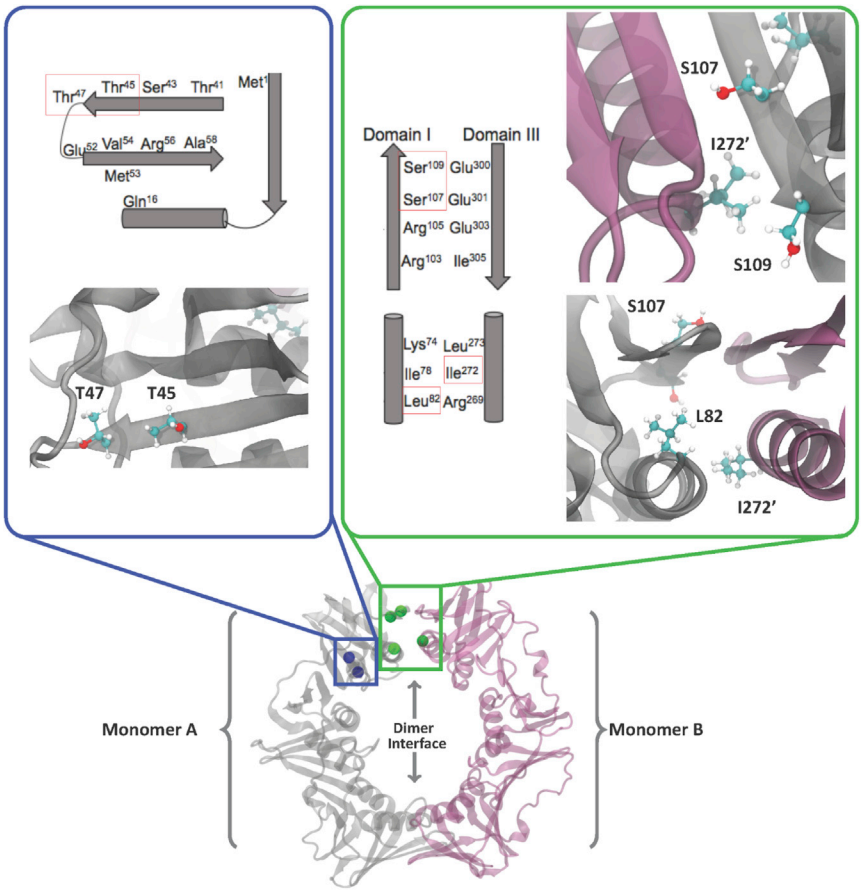

FIGURE 1 Design of β-clamp mutations to stabilize or destabilize the dimer interface. Monomer A is depicted in gray and Monomer B in purple on the three-dimensional representations. The locations of mutations in Domain 1 (T45 and T47 variants) are depicted with blue beads, while the mutations at the dimer interface (L82D, L82E, L82E I 272A, S107R, and S109R variants) are depicted with green beads on the protein.

by ~5000-fold and 100-fold, respectively (12–15). Clamp proteins slide on DNA and serve as platforms for multiple proteins to bind. The β-clamp interacts with all five *E. coli* DNA polymerases (16–26) and coordinates the polymerase switch during translesion synthesis (27–29). In addition, β interacts with replication initiation factors DnaA (30) and Had (31); mismatch repair proteins MutS and MutL; and DNA ligase A, which is responsible for Okazaki fragment maturation (16). Client interactions occur on the front face of the clamp at the 3′ recessed end of DNA at primer-template junctions.

Clamps are loaded on DNA by clamp-loader complexes, which are members of the AAA+ family ATPases (32–35). The loader functions as a switch (36,37) and first binds ATP to bind to the clamp; ATP hydrolysis is not needed for clamp opening but rather for the clamp-loader ejection from the clamp and DNA (38,39). The *E. coli* clamp loader, the γ-complex, contains one copy of each δ and δ' and three copies of γ or τ subunits. The γ/τ subunits harbor the ATPase function, and once ATP-binding sites are occupied, a spiral arrangement is triggered that complements the right-handed helix of DNA. The rearrangement of the clamp loader exposes a region of the δ subunit previously occluded by δ' and allows binding of δ to the β-clamp and the primer-template DNA (40). Available structural data of the γ-clamp-loader complex in its inactive state show an asymmetric conformation and the steric clashes precluding it from binding the clamp (40). The structure of the γ-complex bound to DNA demonstrates the active conformation of a symmetrically aligned clamp loader with all three ATP-binding sites occupied, elucidating the mechanism of ATP hydrolysis induced by the γ-complex binding DNA (41).

The stability of clamps as closed structures varies in different organisms, and trimers tend to be less stable than dimers (42–45). The ability of a clamp loader to open a clamp is determined by the stability of the clamp ring structure. The T4 bacteriophage clamp gp45 tends to be open in solution and unload readily from DNA as a trimer and monomerize (42–46), eliminating the need for the clamp loader gp44/62 to open the clamp. Heterotrimeric *Sulfolobus solfataricus* PCNA samples ring-open states in solution in the absence of its loader (47). The human clamp PCNA is less stable in solution than its nearly identical structural homolog from *Saccharomyces cerevisiae* (48). Evidence exists both for and against opening of yeast PCNA by its replication factor C (RFC) loader complex. It has been shown experimentally that PCNA opening is enhanced by ~20,000-fold when bound to the RFC complex compared to unbound PCNA (49–52). However, computational modeling of a mutated RFC that is unable to form a spiral

arrangement appears to stabilize the open conformation of PCNA rather than destabilize its closed conformation (53). Human PCNA and the β-clamp have been shown to dissociate slowly from DNA, with $t_{1/2}$ of 24 and 60 min, respectively (42). The β-clamp forms a dimer with a K_D of 65–∼600 pM at a concentration three orders of magnitude lower than yeast PCNA (52,54), making the β-clamp the most stable clamp in solution and suggesting the need for clamp opening by the clamp loader. Other work indicates that Domain 1 at the dimer interface can undergo local unfolding in solution, suggesting that at least transient spontaneous opening is possible (55,56).

In dimeric β, the helix harboring residues I272 and L273 of Domain 3 is unwound and distorted to facilitate a hydrophobic interaction with Domain 1 of the other β monomer to create a well-packed dimer interface (Fig. 1). The crystal structure of a monomeric β-clamp (β I272A L273A) bound to the δ subunit of the γ-complex reveals that this helix is undistorted, and the formation of a well-packed dimer interface is prevented (57). In addition, a five-residue loop (274–278) that is part of a turn in the dimeric β structure and therefore occluded from interaction with δ in the closed clamp provides an interaction surface for δ and monomeric β (57). Although δ does not directly interact with the dimer interface of closed β, the above rearrangements are attributed to the interaction of δ with monomeric β. The δ subunit does not open β at the dimer interface but rather stabilizes one monomer, preventing ring closure. The strained conformation of the clamp monomers held together by interactions at the dimer interface can provide the energy for δ to induce β to open or trap β in an open conformation. The monomeric β shows greater flexibility in solution compared to the dimeric structure in HXMS experiments (55), and this dynamic behavior is confirmed by steered molecular dynamics (MD) simulations (58). The simulated monomeric β is dynamic and opens more in solution relative to the dimer. The tilt observed in Domain 3 relative to the other domains of the monomeric clamp is the same as in the crystal structure of the monomeric β-δ complex. Fluorescence-based experiments show that clamp binding is fast, whereas clamp opening is a slower process that does not require ATP hydrolysis (39). The δ subunit alone or the γ-complex depleted of ATP has been shown to unload dimeric β in vitro (59). Binding to δ stabilizes the open conformation, shifting the equilibrium between closed and open β toward an open conformation (57,58).

We previously found that the β-clamp undergoes opening transitions in solution and occupies conformational states in which Domain 1 of β is particularly dynamic, undergoing local cooperative unfolding (55,56). These findings, along with other work demonstrating that β is flexible and under tension in the dimeric state, suggest that β may transiently sample multiple conformations, some of which could be more favorable for clamp-loader binding. The goal of this study is to better understand how the stability of the β-clamp dimer interface influences its dynamic properties and the opening and closing of its ring structure underlying clamp loading. We made a broad set of mutations aimed at stabilizing the closed conformation or destabilizing the dimer interface. Biochemical, biophysical, and computational analyses reveal correlations between dimer stability and clamp opening and loading functions of the β-clamp variants.

MATERIALS AND METHODS

Protein expression and purification

The *dnaN* gene encoding the β-clamp was previously cloned into pET11T and expressed and purified generally as described (55). Detailed methods can be found in the Supporting Materials and Methods. Mutations in this construct were introduced using the QuikChange II Site-Directed Mutagenesis Kit (Agilent Technologies, Santa Clara, CA). Mutations were confirmed by DNA sequencing (Eton, Charlestown, MA). The γ-clamp-loader complex was expressed and purified as previously described (41).

For isothermal titration calorimetry (ITC) experiments, the *dnaN* gene and a fragment of the *holA* gene encoding the N-terminal domain of the *E. coli* γ-clamp-loader complex δ subunit (residues 1–140; referred to as mini-δ) were subcloned into the pET28b+ vector (Novagen, Darmstadt, Germany) using the NdeI and XhoI sites, as described elsewhere (60). Point mutations in the β-clamp gene, encoding T45R, T47R, S107R, S109R, L82D, L82E, L82E I272A, and I272A L273A, were introduced following the modified inverse PCR procedure (61). The nucleotide sequence of the resulting constructs was confirmed by sequencing (Genewiz, Cambridge, MA). Recombinant mini-δ, wild-type (WT) β, and variant β-clamps T45R, T47R, S107R, S109R, L82E, L82E I272A, and I272A L273A were expressed and purified as described previously (60) and in the Supporting Materials and Methods. The β-clamp L82D variant could not be purified in sufficient amounts for ITC experiments.

To test for a potential interaction between β and SSB, *E. coli* BL21 (DE3) strain containing pEAW134 (a gift from Dr. Michael Cox from the University of Wisconsin, Madison) expressing single-stranded DNA binding protein (SSB) (62) was transformed with pET28b expressing His-tagged β-clamp. Transformants were selected on Luria broth plates supplemented with ampicillin and kanamycin. A 50-mL starter culture in a shake flask (200 rpm) was grown overnight at 37°C. A 1-L culture was seeded and grown at 37°C until OD_{600} of 1.0 was reached. Protein expression was induced with isopropyl β-D-1-thiogalactopyranoside to a final concentration of 1 mM at 30°C for 4 h. Cells were harvested by centrifugation for 10 min at 6750 × *g* at 4°C and frozen at −80°C or lysed immediately. Protein overexpression was confirmed by sodium dodecyl sulphate-polyacrylamide gel electrophoresis (SDS-PAGE). Affinity chromatography was used to investigate possible β and SSB interactions (63,64). Cell pellets containing overexpressed β and SSB were resuspended on ice in 50 mM HEPES (pH 7.5), 500 mM NaCl, 30 mM imidazole, 1 mM dithiothreitol, 15% glycerol (buffer A) supplemented with lysozyme and +/− DNase I. Cells were lysed by repeated freeze/thaw cycles (−80°C followed by 37°C). Cell debris was pelleted by centrifugation at 14,000 × *g* at 4°C for 1 h. The lysate was loaded onto a 2 × 5 mL HisTrap HP (GE Healthcare, Marlborough, MA) column and eluted with buffer A and increasing imidazole concentration to 0.5 M. Fractions were analyzed by SDS-PAGE.

Differential scanning fluorimetry

The melting temperature of the WT and variant β-clamps was determined using a thermofluor-based assay (56,65). Optical 96-well clear PCR plates (Thermo Fisher Scientific, Waltham, MA) were used to analyze the melting temperature (T_m) of β proteins. Samples containing 5 μM β protein and a final concentration of 10× Sypro Orange dye (Invitrogen, Carlsbad, CA)

were prepared in a 20-μL reaction volume containing 20 mM HEPES (pH 7.5). The plates were sealed with an optical adhesive film (Applied Biosystems, Foster City, CA). The temperature in a CFX 96 Real-Time System (Bio-Rad, Hercules, CA) was raised from 4 to 100°C in 0.2°C increments every 10 s, and the fluorescence was detected. Samples were analyzed three times in duplicate, and average T_m and standard deviations are reported.

Native and denaturing PAGE

Purified WT β and variants (1 μg each) were incubated in 1× loading buffer (62.5 mM Tris-HCl (pH 6.8), 0.01% Bromophenol Blue, 2.5% β-mercaptoethanol, 10% glycerol) before loading onto 12% PAGEr precast gels (Lonza, Basel, Switzerland) for native PAGE. Proteins were incubated in loading buffer supplemented with 2% SDS at 95°C for 10 min before loading on 16% SDS-PAGE. Gels were stained with Coomassie gel stain.

Native nESI-TIMS-MS

Ion mobility mass spectrometry (MS) experiments were performed on a custom built nanoelectrospray ionization (nESI)-trapped ion mobility spectrometry (TIMS) unit coupled to an Impact Q-TOF mass spectrometer (Bruker, Billerica, MA) (66,67). The TIMS unit is run by custom software in LabView (National Instruments, Austin, TX) synchronized with the MS platform controls (67). Aliquots (10 μL) of WT and clamp variants, dissolved in 10 mM NH_4Ac (native conditions) to 5 μM, were loaded in a pulled-tip capillary biased at 1500 V to the MS inlet. Briefly, the ion mobility separation in a TIMS device is based on holding the ions stationary using an electric field (E) against a moving buffer gas (68). TIMS separation depends on the gas flow velocity (v_g), elution voltage ($V_{elution}$), ramp time (t_{ramp}), and base voltage (V_{out}) (66). The mobility, K, is defined by

$$K = \frac{v_g}{E} \cong \frac{A}{(V_{elution} - V_{out})}. \quad (1)$$

The mobility calibration was performed by varying the ramp time to determine $V_{elution}$ as described (69). The mobility calibration constant A was determined using known reduced mobilities of Tuning Mix components from Agilent analyzed under the same experimental conditions. TIMS experiments were carried out using nitrogen (N_2) as a buffer gas at ambient temperature (T), with v_g set by the pressure difference between the funnel entrance (P1 = 2.6 mbar) and exit (P2 = 1.1 mbar). A radio frequency voltage of 200 V_{pp} at 880 kHz was applied to all electrodes. Ions were softly transferred and injected into the TIMS analyzer section injection to avoid collisional induced activation (i.e., $V_{deflector}$ = 80 V, $V_{capillary}$ = 70 V, $V_{funnel\ in}$ = 0 V, and V_{out} = 60 V; TIMS cell schematic shown in Fig. S1). The measured mobilities were converted into collision cross sections (CCSs, Å^2) using the Mason-Schamp equation:

$$\Omega = \frac{(18\pi)^{1/2}}{16} \frac{q}{(k_B T)^{1/2}} \left(\frac{1}{m} + \frac{1}{M}\right)^{1/2} \frac{1}{N} \times \frac{1}{K}, \quad (2)$$

where q is the ion charge, k_B is the Boltzmann constant, N is the gas number density, m is the ion mass, and M is the gas molecule mass (68).

ITC

The interaction between the WT β or variant clamps with mini-δ was analyzed by ITC performed at 25°C (20°C for L82E, L82E I272A, and I272A L273A β variants) on a Nano-ITC (TA Instruments, New Castle, DE). The ITC experiment consisted of 20 × 2.5 μL injections of mini-δ (0.6–0.7 mM) to the β-clamp solution (0.1 mM) repeated with 300 s interval between injections. The ITC data were corrected for heat measured in corresponding blank titrations of mini-δ into buffer. The data were analyzed using the NanoAnalyze software (TA Instruments) to obtain the dissociation constant K_D, association enthalpy ΔH, and binding stoichiometry parameter n.

ATPase assay and clamp loading assay

The ATPase assay was performed as per the BIOMOL Green manual (Enzo Life Sciences, Farmingdale, NY). The clamp loading assay was carried out by separating biotinylated-DNA-bound proteins from unbound proteins using streptavidin magnetic beads (NEB, Ipswich, MA). Both assays are described in detail in the Supporting Materials and Methods.

Complementation assay

Chemically competent *E. coli* MS120 strain (70) bearing temperature-sensitive mutations in the chromosomal *dnaN* gene was transformed with pET11T empty vector, plasmid encoding WT, or variant β-clamp using a standard transformation procedure (71). After outgrowth at 30°C, cells were plated on Luria broth agar plates in triplicate, supplemented with ampicillin, and grown at 30 or 37°C for 16–18 h. Experiments were repeated three times. Average colony-forming units and standard deviations are reported. Despite the likely low level of expression with pET vectors, β expressed from pET11T is found to complement a $dnaN^{Ts}$ strain and was detected by immunoblot. Indeed, we previously observed sufficient expression from a pET vector of replication protein DnaE to complement a strain harboring a temperature-sensitive allele of *dnaE* (72).

MD simulations

Seven different systems were prepared using the x-ray crystallographic structure of the *E. coli* DNA polymerase III β subunit (Protein Data Bank [PDB]: 1MMI) (8) containing two monomers (A and B) and subjected to MD simulations. The residues that are located on Monomer B are depicted with a prime sign. Each monomer within the proteins contains three different domains that are named alphanumerically with capital "D" and the domain numbers, D1, D2, and D3. The domains on Monomer B are indicated with a prime sign as D1′, D2′, and D3′.

The topology and coordinate files were built after hydrogenation of the samples using the tLEaP module in AMBER16 (73). All of the amino acids were protonated in aqueous solution (TIP3P water), and the ff14SB forcefield parameters were used to model the amino acids (74). The total charge of the WT protein was −22, the total charge of the variants containing negatively charged amino acid (Asp and Glu) mutations was −24, and the total charge of the variants containing Arg mutations was −20. To neutralize the total negative charge of the samples, potassium counterions were added. The waters in the crystallographic structure were deleted, and the system was solvated using TIP3P water molecules. The distance between the solute and the edge of the box was chosen as 12 Å, resulting in an average box dimension of 118.7 × 84.0 × 128.2 Å.

All simulations were performed using the CUDA version of the AMBER 16 pmemd program (73,75,76). Berendsen temperature coupling (77) was employed, and a time step of 1.0 fs was used in all simulations. Periodic boundary conditions were imposed on the samples, and the particle mesh Ewald summation technique (78) was used with 8-Å cutoff distance. The SHAKE algorithm (78) was used for the bonds involving hydrogen atoms. The systems were equilibrated with an 11-stage process after a 1000-step minimization for each system. First, a 10-ps MD simulation was performed at 10 K using a harmonic restraint of 250 kcal/mol/Å^2 on all residues. Second, the harmonic restraint was reduced to 100 kcal/mol/Å^2 in a simulation of 10,000 steps at 10 K. In the third and fourth stages, the harmonic restraints were reduced by half in simulations, each of which were 20 ps at the

same temperature. Fifth, the temperature was gradually increased to 300 K in a 10-ps simulation using a harmonic restraint of 500 kcal/mol/Å^2. Sixth, a 40-ps simulation was performed at 300 K using the same harmonic restraint for all systems. Seventh, the restraints were reduced to 250 kcal/mol/Å^2 in a 20,000-step simulation, which was followed by eighth, another 20,000 steps of simulation with a harmonic restraint of 100 kcal/mol/Å^2 for each system. The ninth and 10th stages were performed with the same harmonic constraints as in the third and the fourth stages, respectively, but at 300 K with 20-ps-long simulations for both stages. Finally, 11th, a 20-ps simulation was performed without harmonic restraints at 300 K. Production simulations were performed in the NVT ensemble at 300 K. Seven different MD trajectories were simulated, each of which was 100 ns.

Trajectory analysis and visualizations

Root mean-square deviation (RMSD), root mean-square fluctuations (RMSFs) of the residues, dynamic cross-correlation analysis, and hydrogen-bond analysis of the trajectories were performed using the cpptraj module (79). All three-dimensional representations were obtained using VMD (80), and the two-dimensional representations were prepared using MarvinSketch (http://www.chemaxon.com) (81).

RESULTS

Motivations for this study and design of the β-clamp variants

The ability of clamp proteins to open and close is essential to their function as protein hubs for recruitment of interacting protein partners that regulate traffic on DNA during replication and repair (2). The dimer interface of the *E. coli* β-clamp is stabilized by four antiparallel β-strands and two α-helices, yet there is evidence that the β-clamp undergoes opening events and populates conformational states in which Domain 1 at the dimer interface in particular is dynamic (55). Several hydrophobic residues line the dimer interface, and previous attempts to destabilize the interface to a considerable extent have proven unsuccessful, except for the double mutation I272A L273A, which is a monomer at low micromolar concentrations (55,82). The β-clamp point-mutation variants F104W, F106A, F106W, and L273A are dimers in solution (82–84). Newer work suggests that electrostatic interactions play a key role in stabilizing the interface (52,54). Our goal in this work was to design and characterize mutations at the dimer interface to test the hypothesis that the clamp transiently populates open conformational states captured by the high-affinity binding by the clamp loader in the process of clamp loading.

Our approach included constructing a broad range of mutations altering the stability of the dimer interface (Fig. 1). Starting with the crystal structure of the clamp (4,8) as a guide, we chose a set of amino acid substitutions with the goal of either stabilizing or destabilizing its dimeric structure. We avoided making mutations at L273 because this residue lies on the side of the β-clamp involved in binding DNA polymerases and the clamp loader and could interfere with these interactions. Furthermore, we designed mutations away from residues E93 and L98 because they are important for interactions with DinB and UmuC (26,85–87).

To weaken the dimer interface, we introduced charge at residue L82, specifically L82D and L82E, to remove existing hydrophobic interactions and increase the repulsion at the dimer interface. Additionally, we combined the L82E mutation with an I272A mutation that replaces a larger hydrophobic residue with a smaller one. We hypothesized that mutating S107 and S109 to charged arginine residues would cause the formation of a salt bridge across the dimer interface and thereby stabilize the β-sheet at the dimer interface. Furthermore, we wanted to stabilize Domain 1 of the clamp to reduce the conformational flexibility we previously observed in this region. In the hydrogen-deuterium exchange mass spectrometry (HXMS) experiments, we observed increased deuterium uptake, consistent with β transiently populating open states in which Domain 1 is more flexible and prone to unfolding. Indeed, the peptide including residues 1–34 exhibited EX1 kinetics, indicating local unfolding in that region of the clamp (55,56). Thus, we made mutations near this region, introducing charged Arg at positions T45 and T47 to increase ionic interactions with E52 and stabilize β-strand 4 and α-helix 1. Although these mutations likely stabilize Domain 1 in the context of both the closed state and the open states with disrupted dimer interface, we expect they also increase stability of the β dimer by reducing the entropic penalty associated with the loss of Domain 1 flexibility upon formation of the closing ring.

Thermostability gives insight into the effect of dimer interface mutation

To assess whether we had altered the thermostability of the resultant variant clamps, we used a thermofluor assay, in which WT and variant β-clamp proteins incubated with a fluorescent dye were subjected to increasing temperatures. Initially, no fluorescent signal is observed because the fluorescence of the dye is quenched by water, but as the protein denatures, more of its hydrophobic regions are exposed and more dye binds until maximal fluorescent signal is reached (Fig. 2 *A*). From this, we can calculate the melting temperature of the protein, which is defined as the temperature at which 50% of the protein is unfolded. A stabilizing mutation is expected to increase the melting temperature of the protein, and a destabilizing mutation is expected to decrease the melting temperature. Indeed, all mutations that were designed to be stabilizing, namely T45R, T47R, S107R, and S109R, have melting temperatures similar to or a few degrees higher than WT β (69.0°C) (Fig. 2 *B*). Compared to WT β, β L82D and β L82E I272A have significantly lower melting temperatures of 49.5 and 45.3°C, respectively, whereas the L82E mutation more modestly decreases the melting temperature to 62.3°C. Overall, following the above strategy, we have successfully designed a set of

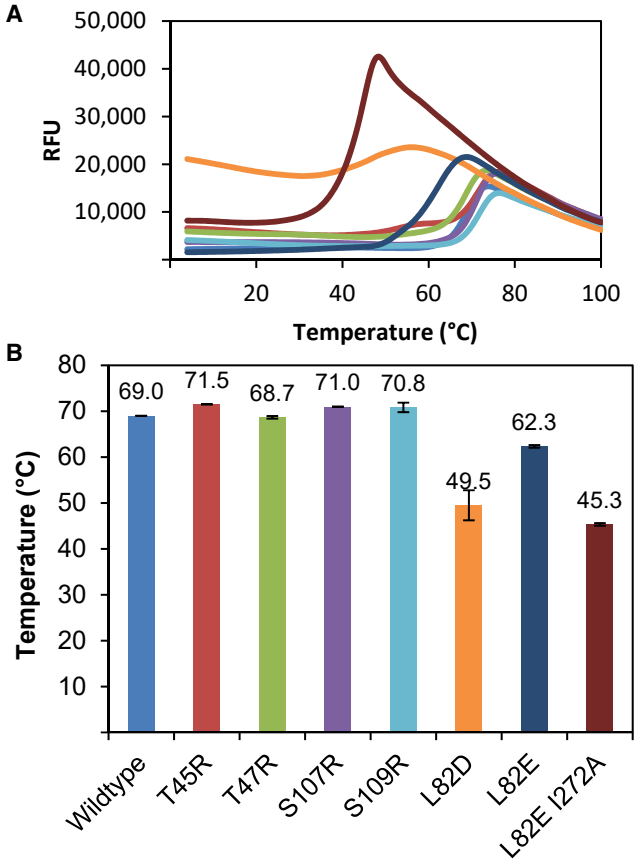

FIGURE 2 (*A*) Differential scanning fluorimetry of WT and variant β-clamps. Melting temperatures were observed by monitoring Sypro Orange dye fluorescence. (*B*) Bar graph showing average melting temperatures and standard deviations for WT β (*light blue*), β T45R (*red*), β T47R (*green*), β S107R (*purple*), β S109R (*cyan*), β L82D (*orange*), β L82E (*dark blue*), and β L82E I272A (*maroon*) from triplicate experiments.

both stabilizing and destabilizing β-clamp mutations that we subsequently use to correlate the β-dimer stability with opening dynamics, clamp-loader binding, and loading efficiency.

Native gel electrophoresis and native nESI-TIMS-MS shows altered dimerization state of variants

A representative denaturing gel (Fig. 3 *A*) shows the purity of WT and variant β-clamps and monomeric conformations on SDS-PAGE. The dimerization state of WT and variant β-clamps was evaluated by native gel electrophoresis (Fig. 3 *B*). WT β and the T45R, T47R, S107R, and S109R variants have a pronounced dimer band, whereas mutations at position L82 only or when in combination with I272A result in a less prominent dimer band. Indeed, the L82D variant shows a very weak dimer band and instead shows mainly monomeric and multimeric conformations, which are presumably monomers forming multimeric structures.

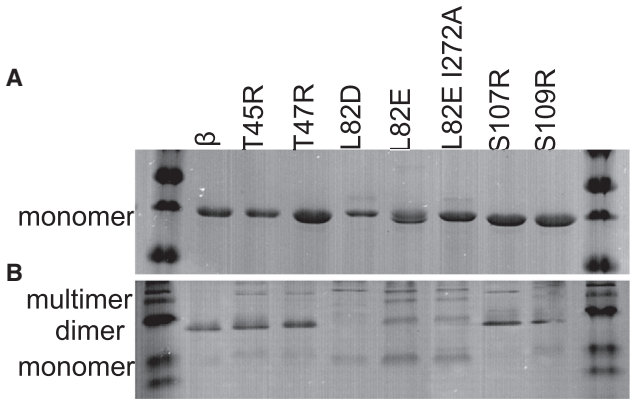

FIGURE 3 Native gel electrophoresis to assess dimerization state of variants. (*A*) Denaturing PAGE showing purified WT and variant clamp proteins as monomers in the presence of SDS. (*B*) Native PAGE shows monomeric, dimeric, and multimeric conformations of WT and variant clamp proteins at 1 μg each.

Mass spectra of the WT β-clamp and the L82E variant displayed a major dimer distribution, ranging from $[M + 16H]^{16+}$ to $[M + 20H]^{20+}$ (Fig. 4, *A* and *B*; Table S1), and a minor tetramer distribution, ranging from $[M + 25H]^{25+}$ to $[M + 28H]^{28+}$ and $[M + 24H]^{24+}$ to $[M + 28H]^{28+}$, respectively (Fig. 4; Table S1), when using native nESI. In the case of the L82E I272A variant, the mass spectrum displayed an equivalent monomer and dimer distribution, ranging from $[M + 10H]^{10+}$ to $[M + 12H]^{12+}$ and $[M + 16H]^{16+}$ to $[M + 19H]^{19+}$, respectively (Fig. 4 *C*; Table S1). However, only a monomer distribution, ranging from $[M + 10H]^{10+}$ to $[M + 12H]^{12+}$, was obtained in the MS spectrum of the L82D variant (Fig. 4 *D*; Table S1). These MS data were thus found consistent with our other observations indicating that the L82E I272A and L82D variants destabilize the clamp structure, whereas the glutamic acid mutation at residue L82 (L82E) does not disrupt the clamp as much. Typical TIMS spectra for the multiply protonated species of the *n*-mers of the clamp variants are shown (Fig. 4), and the measured CCSs are listed in Table S1. Inspection of the TIMS spectra for dimers and tetramers of the WT clamp exhibited higher CCS values as compared to the dimers and tetramers of the L82E variant for the same charge states. This means that the additional negative charge provided by the L82E mutation leads to a more compact conformation than the WT clamp, probably by making additional hydrogen bonds around the mutation site (see below, MD Simulations). In addition, the presence of some dimers for the L82E I272A variant at similar CCS values, as compared to the L82E variant dimers, suggests that the hydrogen-bond network is only partially perturbed by substituting a larger hydrophobic residue with a smaller one. Furthermore, the observation of only monomers for the L82D variant at similar CCS values, as compared to some monomers observed for the L82E I272A variant,

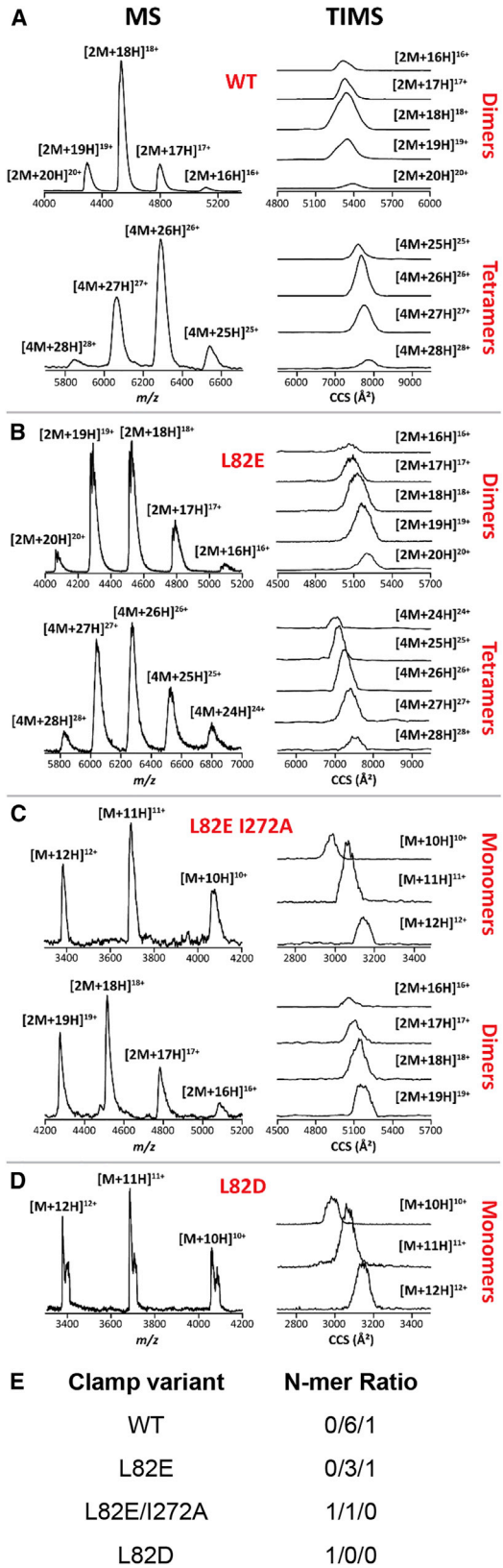

FIGURE 4 MS and TIMS spectra for the multiply protonated species of the β-clamp (*A*) WT, (*B*) L82E, (*C*) L82E I272A, and (*D*) L82D variants. (*E*) The distribution of monomers/dimers/tetramers (Table S1). To see this figure in color, go online.

suggested that the two monomer variant structures adopt similar conformations despite the different mutations. The native TIMS-MS experiments enabled us to conclude that the mutation most responsible for the disruption of the dimers is provided by the negatively charged L82D, in which the hydrogen-bond network is strongly perturbed around the mutation site as compared to the L82E and L82E I272A variants in the gas phase. Our observations from native gel electrophoresis and TIMS-MS indicate that WT β, the stabilizing T45R, T47R, S107R, and S109R variants, and the moderately destabilizing β L82E variant remain dimeric at micromolar concentrations, whereas β L82E I272A and β L82D are at least partially monomeric.

Designed β variants bind mini-δ with affinity similar to that of WT β

To probe the effect of altered stability of the β-clamp variants on their affinity for the clamp-loader complex, we characterized interaction of mini-δ with WT β; with the stabilizing variants β T45R, β T47R, β S107R, and β S109R; and with the destabilizing variants β I272A L273A, β L82E, and β L82E I272A using ITC. Note that we were unable to express and purify the least stable variant, β L82D, in the amount necessary for ITC binding studies with mini-δ. The raw ITC data and the fits for the β-clamp variants are shown in Fig. S2. The binding parameters for mini-δ with all considered β-clamp variants, including the equilibrium dissociation constant K_D, association enthalpy ΔH, binding stoichiometry parameter n, and association entropy ΔS, are listed in Table 1.

Previous studies demonstrated that the equilibrium dissociation constant K_D for δ binding to WT β (determined by surface plasmon resonance) is one to two orders of magnitude weaker than the K_D for δ binding to β I272A L273A (82);

TABLE 1 Binding Parameters for Mini-δ and β-Clamp Variants Obtained by ITC

β-clamp variant	K_D (μM)	n	ΔH (kJ/mol)	ΔS (J/mol/K)	T (°C)
WT	5.6 ± 0.69	1.01 ± 2.0×10^{-4}	−21.6 ± 0.4	27.7	25
I272A L273A	0.53 ± 0.08	0.71 ± 0.01	−34.6 ± 0.4	2.0	20
L82E	6.6 ± 1.8	0.83 ± 0.03	−17.8 ± 1.1	38.6	20
L82E I272A	5.5 ± 1.0	0.41 ± 0.01	−34.0 ± 2.0	−15.3	20
S107R	4.4 ± 0.9	0.96 ± 0.02	−20.4 ± 0.8	34.2	25
S109R	5.0 ± 1.1	1.06 ± 0.03	−19.4 ± 0.9	36.5	25
T45R	6.7 ± 2.0	0.95 ± 0.03	−22.5 ± 1.5	23.4	25
T47R	6.0 ± 1.7	0.95 ± 0.03	−22.5 ± 1.4	24.3	25

Mini-δ (0.6–0.7 mM) was titrated into 0.1 mM β-clamp solution. The parameters include the dissociation constant K_D, association enthalpy ΔH, binding stoichiometry parameter n, and association entropy ΔS obtained at 25°C (20°C for L82E, L82E I272A, and I272A/L273A β variants).

therefore, this variant was included here as a control. We were able to confirm this result by ITC (Fig. S2; Table 1): titration of mini-δ into a solution of WT β resulted in a K_D of $\sim$6 μM, whereas K_D for mini-δ binding to β I272A L273A was 0.5 μM, over one order of magnitude stronger. Furthermore, the association enthalpy for β I272A L273A was $\sim$1.6-fold higher than for WT β (ΔH of -35 kJ/mol vs. -22 kJ/mol for WT β). It is remarkable that mini-δ binding to WT β also resulted in positive (favorable) change in entropy (ΔS $\sim$28 J/mol/K), presumably due to dehydration of the binding interface accompanied by an increase in solvent entropy. On the other hand, the association entropy for mini-δ binding to β I272A L273A was much smaller than for WT β (ΔS $\sim$2.0 J/mol/K). This is consistent with higher flexibility of the I272A L273A β mutant, presumably due to increased sampling of a more dynamic open conformation, which is reduced upon mini-δ binding.

On the other hand, ITC analysis for mini-δ binding to stabilized β variants T45R, T47R, S107R, and S109R resulted in K_D values of 4–7 μM and ΔH about -20 kJ/mol, similar to those obtained for mini-δ binding to WT β. However, the association entropy for two of the stabilized variants (S107R, S109R; ΔS $\sim$34–37 J/mol/K) was slightly higher than for WT β (ΔS $\sim$28 J/mol/K), potentially pointing to a smaller entropic penalty associated with a decrease in β-clamp flexibility upon mini-δ binding.

Interestingly, the K_D (6.6 μM) and association enthalpy and entropy (ΔH $\sim$ -18 kJ/mol and ΔS $\sim$39 J/mol/K, respectively) obtained for the destabilized L82E variant are similar to those for β S107R and β S109R, likely suggesting that at the concentrations used in our ITC measurements ($\sim$100 μM), β L82E predominantly resides in the closed state. However, β L82E I272A, although displaying only a marginally stronger K_D (5.5 μM), shows similar trends as β I272A L273A, i.e., higher association enthalpy than for WT β (ΔH of -34 kJ/mol vs. -22 kJ/mol) and a much smaller association entropy (ΔS of -15.3 J/mol/K vs. 28 J/mol/K). These ITC data suggest that stabilizing (T45R, T47R, S107R, S109R) and moderately destabilizing (L82E) β variants reside in the closed state at our experimental conditions ($\sim$100 μM β) and exhibit K_D and ΔH for mini-δ binding similar to those observed for WT β. On the other hand, more destabilizing β L82E I272A and β I272A L273A variants increasingly populate open-like conformation(s) and exhibit larger (favorable) association enthalpy ΔH and smaller (less favorable) association entropy ΔS, which is consistent with the formation of more stabilizing intermolecular contacts and greater flexibility loss for open β-clamp upon mini-δ binding.

Lower ATPase activity of the γ-complex is observed in the presence of β L82D and DNA

We next assessed whether the variant β-clamps stimulate the ATPase activity of the γ-complex in the presence of primed DNA, using a colorimetric inorganic phosphate quantitation assay. We incubated each of the reaction components alone or in combination and measured the absorbance to assess color formation; the increase in inorganic phosphate in solution is brought about by the ATPase activity of the γ-complex (Fig. 5 *A*). No significant color change is observed when ATP, β, γ-complex, or DNA alone are incubated in assay buffer or when ATP and γ-complex or ATP, β, and γ-complex are incubated in the absence of DNA. ATPase activity is detected when primer-template DNA is added to ATP, β, and the γ-complex. The β L82D variant does not enhance the ATPase activity of the γ-complex, β S109R shows a modest decrease in conferring enhancement of the ATPase activity, and other variants result in similar levels of ATPase activity compared to the level induced by the presence of WT β-clamp (Fig. 5 *B*). ATP hydrolysis occurs upon release of β on DNA by the γ-complex, so reduced ATPase activity could be due to defects in clamp binding to the loader, clamp loading, or in release of the β-clamp on DNA.

Stabilized variants are efficiently loaded onto primer-template DNA

To evaluate clamp loading of the β variants, we adapted an assay (88) utilizing a 5′ biotinylated primer-template substrate with a 5′ single-stranded overhang for loading of the clamp and streptavidin-coated magnetic beads that allow for separation of bound and unbound protein. To prevent β from sliding off the linear DNA, SSB is added to the loading reactions, which traps β on single-stranded DNA (ssDNA; Fig. S3). After the loading reactions are washed with buffer, bead resuspensions are applied to the magnet, the pellet (P) fractions indicate loaded β, and the supernatant (S) fractions indicate unloaded β, shown at 0 and 60 min.

Representative anti-β immunoblots show the loading efficiencies of the WT and variant β-clamps (Figs. 5 *C* and S3). Overall, the amount of loaded β and the amount still present after 60 min is greater in the variant clamps with intended stabilizing mutations T45R, T47R, S107R, and S109R, as indicated by the greater amount of β in the pellet at 0 and 60 min (Fig. 5 *C*). Less of the L82D variant is loaded on DNA than WT β, whereas the β L82E and L82E I272A variants appear to remain loaded on DNA, as indicated by the absence of β in the supernatant at 0 and 60 min and the presence of β in the pellet at 60 min. These observations could indicate altered interactions with the clamp loader and, in the case of β L82D, are consistent with a less stable β dimer. The ITC experiments (Fig. S2; Table 1), which indicate similar equilibrium dissociation constants for these clamps as for WT β binding to mini-δ, were carried out with only a truncation of the δ subunit of the clamp loader, whereas the ATPase and loading assays are carried out

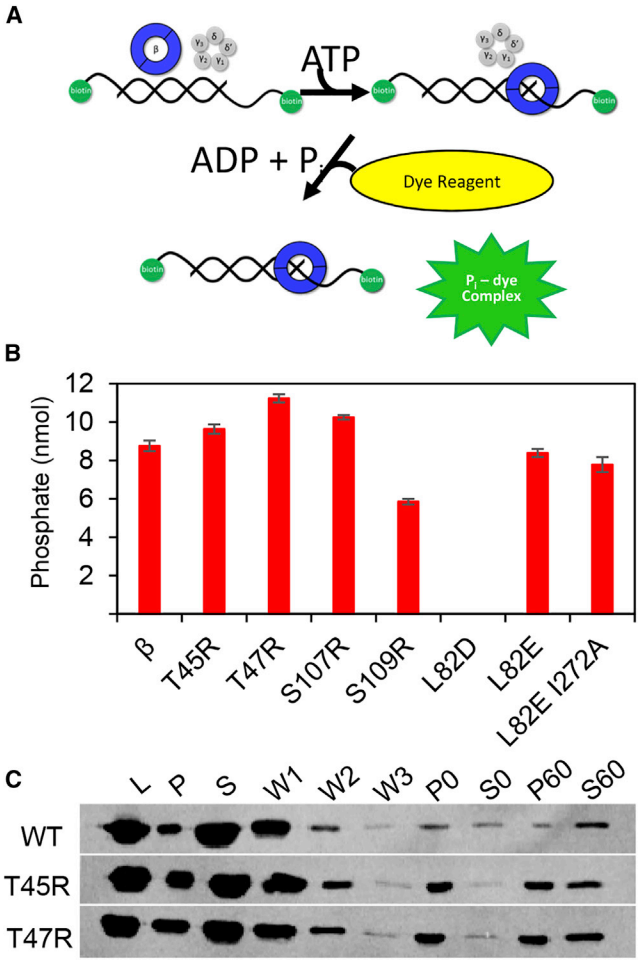

FIGURE 5 ATPase activity of the γ-complex measured using a BIOMOL Green colorimetric reagent. (*A*) A schematic depicting loading of the β-clamp onto a primer-template DNA with biotinylated 5′-ends. The template is longer than the primer, resulting in a 3′ recessed end onto which the γ-complex loads β in the presence of ATP. ATP hydrolysis ejects the clamp loader. The increase of inorganic phosphate following the loading reaction is measured by addition of the BIOMOL Green reagent. (*B*) A bar graph showing the amount of phosphate released (nmol) during the loading reaction after the intrinsic γ-complex ATPase activity is subtracted (γ-complex hydrolyzes ATP in the presence of DNA, β enhances the ATPase activity of the γ-complex). Average nmol of phosphate released and standard deviations from at least three replicates are reported. (*C*) Immunoblot detection of β loaded onto a primer-template substrate using a bead-based assay for WT β and the variants indicated. Input control (L) indicates the amount of β in each loading reaction. After three wash steps (W1, W2, and W3), pellet (P) fractions indicate loaded β and supernatant (S) fractions indicate unloaded β, respectively, for both 0- and 60-min time points (also see Fig. S3)

with the full five-subunit clamp loader. We did not observe in our simulations that the destabilizing β variants have more extensive contacts with DNA than WT β; however, altered or additional hydrogen-bonding interactions at the dimer interface could explain the persistence of the destabilizing β variants on DNA (Fig S3; see below, MD Simulations).

β L82D and β L82E I272A variants do not support cell growth in complementation assay

To determine whether the variant β-clamps support cell growth, we utilized an *E. coli* MS120 strain (70) bearing mutations conferring temperature sensitivity in the chromosomal *dnaN* gene. The MS120 strain grows uninhibited at 30°C but is unable to grow at temperatures of 37°C or higher unless complemented with a functional β gene. We transformed these cells with either empty vector or plasmids expressing WT or variant β-clamps, grew them at 30 and 37°C, and determined the number of colony-forming units at each temperature (Fig. 6). All transformants grew at 30°C, but only those that produced functional clamps were able to support growth at 37°C. The β L82D and β L82E I272A variants did not support cell growth in the complementation assay. Interestingly, the β L82E variant was able to complement growth, but the resultant colonies were much smaller, suggesting these clamps were compromised, resulting in a growth defect. Thus, all stabilizing clamp variants confer growth on the temperature-sensitive strain, whereas the destabilizing variants β L82D, β L82E I272A, and β L82E are unable or less able to rescue growth at the nonpermissive temperature. We analyzed protein levels at the nonpermissive temperature by immunoblotting, which shows that the variants were expressed at detectable levels, except the L82E I272A variant, which does not support growth at 37°C and therefore was not analyzed (Fig. S5).

MD simulations reveal altered conformations and dynamics of β-clamp variants

MD simulations with WT β-clamp and the seven variants were performed to evaluate the effect of the mutations on the dynamics of the protein. The stability of the trajectories has been investigated with RMSD analysis of the backbone atoms (C, C_α, and N) of β on Monomers A and B separately. In all cases, the average RMSD for both the full-length protein and backbone atoms on Monomers A and B was at or below 3 Å (Figs. S6 and S7).

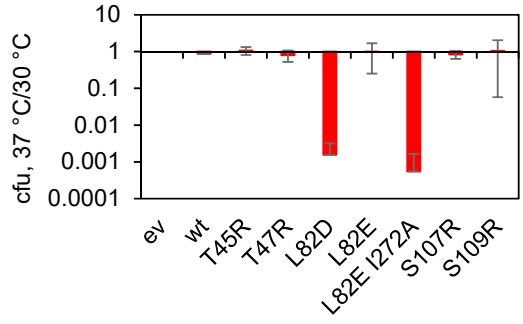

FIGURE 6 Ratio of colony-forming units at 37°C vs. 30°C for WT and variant β-clamps in complementation assay. EV indicates the empty vector. Data represent the average and error bars represent the standard deviation of at least three replicates. To see this figure in color, go online.

Changes in RMSF relative to WT β were determined to assess the effect of the point mutations on the fluctuations for the different variants. Nine residues with a change in relative RMSF value greater than ± 1 Å were observed for the different variants (Fig. S11). P20′, L21′, and G22′ on Monomer B (indicated by the *prime symbol*) become more mobile in the L82E variant (Fig. S11, *green*) relative to WT β. D120′, which is located on the interdomain connector loop between D1 and D2, becomes more mobile in the S107R variant (Fig. S11, *cyan*), whereas the mobility of D120′ is observed to be either very similar to that of the WT protein or calculated to be less than that of WT β for all other variants. The interdomain connector loop has been previously reported to have regions that are rapidly deuterated in HXMS experiments with different clamp proteins (56).

The effect of different point mutations on the correlations between the residues located at the dimer interface was studied by calculating the deviation of the cross correlations with respect to WT β (Fig. S12). Helix-3 (H3) and helix-21 (H21) are observed to be mostly positively correlated in the L82E, T45R, and S107R variants (Fig. S12 *A*, region colors: *blue-cyan*), whereas negative correlations are found for the remaining systems relative to WT β.

For the Domain 3-Domain 1′ interface, helix-10 (H10) and helix-14 (H14) are observed to be correlated in the T45R and S107R variants (Fig. S12 *B*, region colors: *blue-cyan*). The L82E and L82E I272A variants increase the number of residues in β sheets that are correlated with each other on the domain interface between Domain 1 and Domain 3′. The region composed of residues from L82 to R96, in particular, is found to be highly correlated with the region composed of residues Y282′ to N295′ in these variants. It is noteworthy that the magnitude of the correlations between these β-sheets is the highest in the L82E I272A variant relative to the other systems (see Supporting Materials and Methods for detailed results).

The two-dimensional representation of the hydrogen bonds that are observed within the dimer interface based on a hydrogen-bond analysis of the simulations is given in Fig. S15, in which each hydrogen-bond interaction is depicted by a different color. Several changes in the interdomain contacts are observed, depending on the individual mutation. The L82D and L82E variants introduce negatively charged residues into the protein, which alter the hydrogen-bond network around the mutation site. The total fraction of frames that had hydrogen bonds around the mutation site is depicted in Fig. 7. It is observed that the hydrogen bond between the backbone oxygen atom of G81 and the side chain of Q265 of the neighboring monomer is conserved in both interfaces in a higher percentage of the sampled frames of β L82D, whereas the Domain 1-Domain 3′ interface exhibits the interaction for a higher percentage than on the Domain 3-Domain 1′ interface of the β L82E variant (Fig. 7 *A*) relative to WT β. This interaction is conserved with a higher percentage in at least one dimer interface of β L82E I272A variant relative to WT protein (Fig. 7 *A*). There is almost no alteration in these interactions with other mutations. In the WT protein, the backbone oxygen atom of G81 and G81′ forms a hydrogen bond with the side chains of R269′ and R269, respectively (Fig. 7 *B*). However, the L82D variant results in a smaller total fraction of frames with this hydrogen bond present. On the other hand, the L82E variant increases the time this interaction is observed, especially on the Domain 3-Domain 1′ interface.

A similar pattern is seen in the β L82E I272A variant but with longer conservation time on the D1-D3′ interface compared with the Domain 3-Domain 1′ interface. These results indicate that the mutation of L82 to a negatively charged residue, especially Glu, increases the total fraction of time that the backbone oxygen atoms of G81 and G81′ can receive a hydrogen bond from a neighboring residue. The mutations in the T45R and S107R variants also increase the number of frames in which G81 and G81′ have hydrogen bonds with R269′ and R269, respectively, relative to WT β (Figs. 7 *B* and S15).

The most dramatic alteration observed is for the L82D, L82E, and L82E I272A variants, for which a new contact is formed only in these systems and not any other. In these systems, the carboxyl moiety on the side chains (D or E) form hydrogen bonds with the positively charged side chain of R269 and R269′ (Fig. 7, *C* and *D*). This interaction is maintained for at least 60% of the simulation time in the β L82D variant. In the β L82E variant, the two dimer interfaces appear to be asymmetric with respect to hydrogen bonding between residues 82 and 269. The introduction of the additional mutation, I272A, reduces the distinctive feature between the two dimer interfaces of β L82E I272A, in which the interactions are present at least 60% of the simulation time at both dimer interfaces. These results are consistent with the fact that this variant remains loaded on DNA. Similar differential effects at other locations in β are observed for other sites, including R96 and R96′, S109 and S109′, and T45R and T45′R (see Supporting Materials and Methods). As with the cross-correlation analysis, the largest perturbations to hydrogen bonding are found in the destabilizing β L82D, L82E, and L82E I272A variants.

DISCUSSION

Structural and biochemical observations have provided many of the mechanistic details regarding the clamp loading process and reveal variations across species. The crystal structure of *E. coli* γ-complex in its inactive conformation demonstrates its inability to bind to the β-clamp because of steric clashes (40). The crystal structure of the γ-complex with all its ATPase sites occupied bound to DNA reveals its

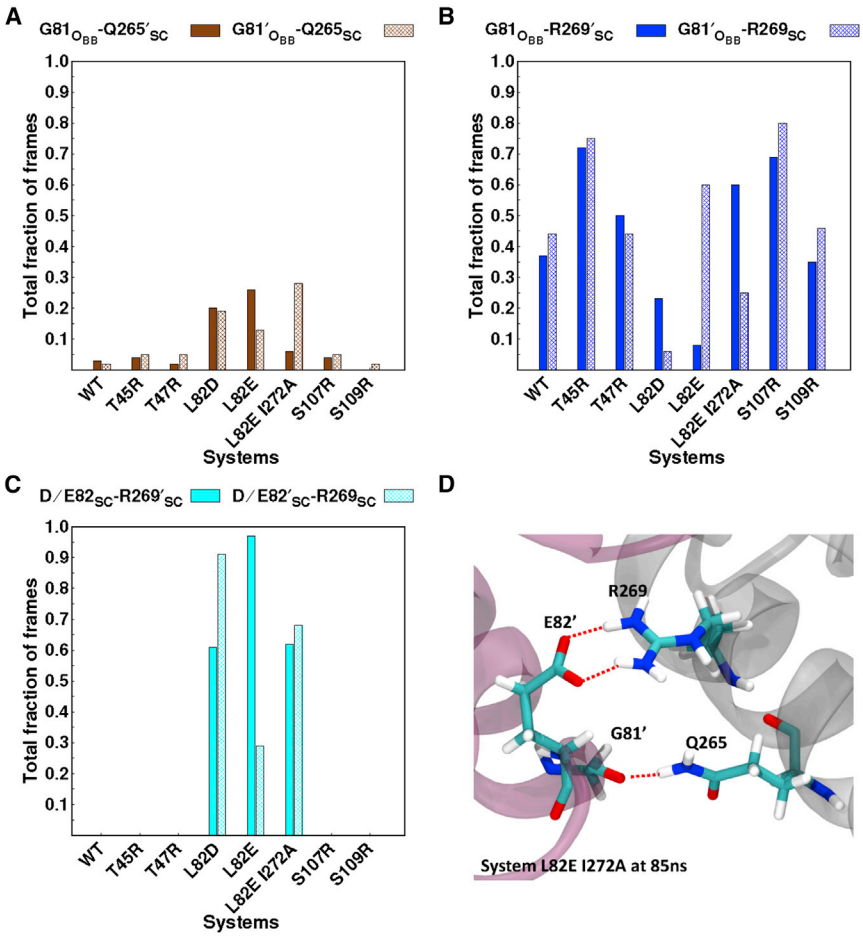

FIGURE 7 The total fraction of the frames that a hydrogen bond exists between (*A*) the backbone oxygen atom of G81 and side chain Q265′ (*solid brown*) and the backbone oxygen atom of G81′ and side chain Q265 (*pattern brown*), (*B*) the backbone oxygen atom of G81 and side chain R269′ (*solid blue*) and the backbone oxygen atom of G81′ and side chain R269 (*pattern blue*), and (*C*) the side chain of D82/E82 and side chain R269′ (*solid cyan*) and the side chain of D/E82′ and side chain R269 (*pattern cyan*). The backbone oxygen atoms are depicted with subscript "O," while the side chain is depicted with subscript "SC." (*D*) The three-dimensional representation of the depicted interactions obtained from the trajectory at 85 ns of variant L82E I272A.

active conformation and the mechanism of ATP hydrolysis (41). However, the conformation of the clamp loader when it binds the clamp is unknown because the crystal structure of the clamp-clamp loader complex has not been solved, possibly because such an intermediate may be short-lived, as the clamp may sample open and closed states in solution.

Clamp-loader-facilitated opening of the clamp can be an active process in which the clamp loader binds a closed clamp and opens it or the clamp loader can bind to and stabilize a transiently open clamp (42–45). The T4 bacteriophage clamp gp45 is frequently open in solution and therefore does not need a dedicated clamp loader for opening; instead, the gp44/62 stabilizes the open conformation (42–46). The crystal structure of the T4 gp45 clamp bound to gp44/62 clamp loader and DNA (89) reveals an open clamp-clamp loader assembly, whereas in the structure of the yeast PCNA-RFC complex, the clamp is closed (90). The yeast closed-clamp structure may be an artifact because an arginine finger variant of the clamp loader was used that renders the loader unable to form a helical conformation and bind the clamp.

The β-clamp has a $t_{1/2}$ of 60 min on DNA (42). In *E. coli*, the δ subunit moderates the affinity of the complex for the clamp (91), and the δ subunit alone has been shown to unload the clamp (59). The δ subunit has been demonstrated to have a higher affinity for the β monomer rather than the dimer, suggesting that δ prefers the open conformation of β (57). The structure of mini-δ bound to a β variant that is not a stable dimer shows a relaxed curvature that results in a ∼15-Å opening at one dimer interface, a distortion wide enough to accommodate ssDNA (57). The δ subunit does not destabilize β at the dimer interface but rather binds to the hydrophobic pocket where most β client interactions occur (57). The helix containing residues I272 and L273 in β Domain 3 is under strain and allows for an intermonomer hydrophobic interaction with Domain 1, forming a tight dimer interface. In the crystal structure of the monomeric β-clamp bound to the δ subunit, these residues are mutated to alanine, and these smaller hydrophobic residues prevent dimer formation in the low micromolar range (57). Furthermore, the five-residue loop immediately following those residues provides an interaction surface for monomeric β and δ, whereas the loop is occluded in dimeric β. The monomer shows more dynamic behavior than WT β in the HXMS experiments (55). This greater flexibility is supported by steered MD simulations as the monomer opens up more relative to the dimer (58), and this region is perturbed most in the β L83E variant (Fig. S11).

A 7° interdomain angle is observed in the simulated monomeric clamp (58), which is similar to the angle observed in the crystal structure of the β monomer complexed to the δ subunit (57).

We previously observed that residues 1–34 in Domain 1 undergo a local cooperative unfolding as they are deuterated faster and display EX1 kinetics in HXMS experiments (55,56). The solvent accessibility of these residues signifies the greater flexibility in this region and suggests that β transiently opens in solution. The crystallographic data, along with HXMS experiments, suggest that the γ-complex traps β in an open conformation as the strain held at the dimer interface is alleviated and the δ subunit serves to prevent ring closure. The δ subunit does not open β at the dimer interface but rather stabilizes one monomer, preventing ring closure. Here, we further investigate the dynamic behavior at the dimer interface and its effect on the opening and closing of the ring structure. Using the crystal structure of WT β as a guide, we designed mutations with the intention of stabilizing or destabilizing the dimer interface.

The mutations we hypothesized to be stabilizing, T45R, T47R, S107R, and S109R, had similar or increased thermostability compared to WT β and similar functions as WT β except for having greater residence on DNA after loading (Fig. 8). The atomic fluctuations that the mutations produced in the MD simulations were examined by performing RMSF analysis. The highest increase in the mobility of residues G209, G210, and D211 was observed in the T45R variant. The same residues on the opposite monomer were less mobile in all other variants except for the T47R variant. The hydrogen-bond analysis of the MD simulations determined that residues R45 and R47 within T45R and T47R variants formed new interactions with E52 relative to WT β (Fig. S17). Additionally, in the S107R variant, R107 formed interactions with E93 (Fig. S20 *E*). Lastly, R96 was observed to interact with Q299 and S107 in the S109R variant (Fig. S20).

The mutations designed to be destabilizing disrupted the dimer interface to varying degrees (Fig. 8). The L82D variant produced the greatest destabilization effect by far, and in comparison, L82E had milder effects. When the L82E mutation was combined with I272A, the effect closely resembled the L82D variant. The β L82D and L82E I272A variants had significantly reduced thermostability, whereas β L82E moderately reduced the melting temperature of the protein by ~7°C (Fig. 8). The dimerization state of all

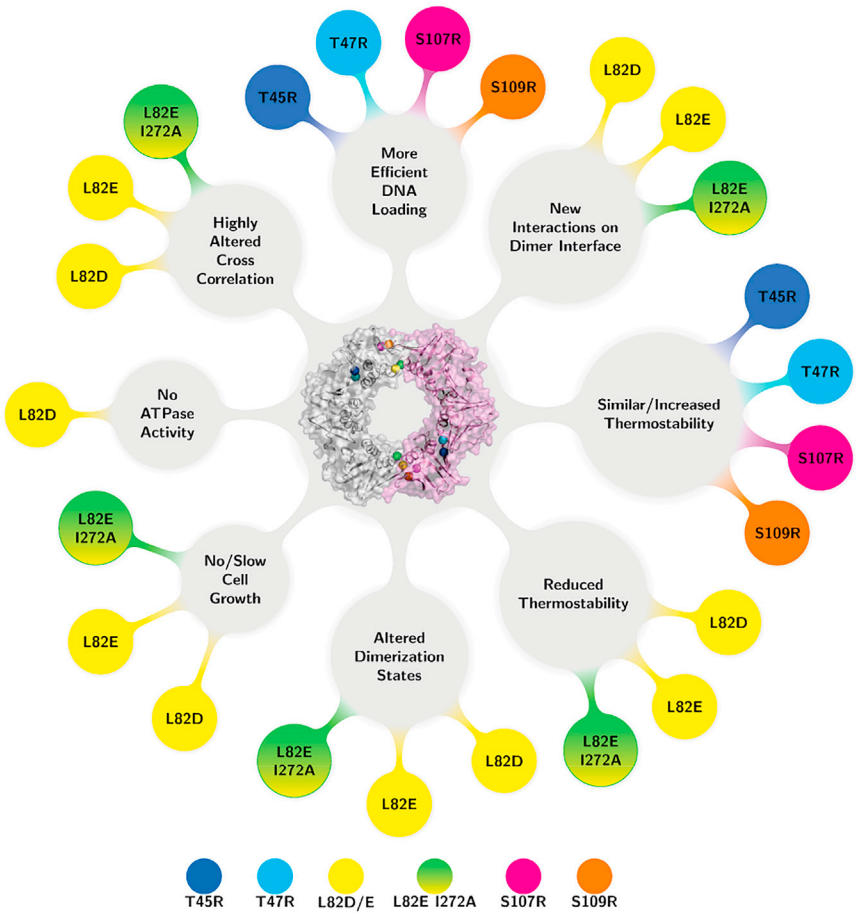

FIGURE 8 Summary of results presented, showing the different effects of each of the mutations made.

three variants was altered, with β L82D detected as a monomer at concentrations in the μM range, β L82E I272A as monomer and dimer, and β L82E as dimer and multimer by native PAGE and native TIMS-MS. The β L82D and β L82E I272A variants did not complement cell growth in the temperature sensitivity assay. The β L82E variant supported cell growth but resulted in smaller colonies that grew to a normal size with longer incubation time. The intrinsic ATPase activity of the clamp loader was not stimulated by the addition of β L82D, whereas β L82E and β L82E I272A stimulated the ATPase activity to nearly the same extent as the WT β-clamp. The destabilized β L82E and β L82E I272A variants did not appear to unload from the linear, end-blocked DNA substrate. One possibility that would explain this observation is that these variants might remain bound to the γ-complex, as the δ subunit has been shown to have greater affinity for an open clamp. The L82E and L82E I272A variants had similar affinity for mini-δ as WT β, but those experiments were carried out only with mini-δ, whereas the clamp-loading experiments were performed with the complete clamp-loader complex and DNA. The β L82D variant did not stimulate the ATPase activity of the γ-clamp loader and was loaded onto DNA less efficiently than WT β. The RMSF of L248, which is in close proximity to the β client protein-binding pocket (19,57,92), was observed to increase in one of the monomers in the L82E I272A variant. P20′, L21′, and G22′ on the second monomer were observed to be more mobile in the L82E variant. These residues are located on the complementary region consisting of residues 1–34, which was previously reported to undergo a local cooperative unfolding and to display EX1 kinetics in the HXMS experiments (55,56). Difference cross-correlation analysis for these destabilizing variants suggests that at least one of the two dimer interfaces (both interfaces in L82D) exhibits higher anticorrelated movement in the interface region compared to WT β, as well as higher changes in correlation overall. The hydrogen-bond analysis revealed that changing the leucine at the 82 position to either an aspartic acid or glutamic acid resulted in new interactions between D/E82 and R269 and between G81 and Q265. These new hydrogen-bond interactions also reduce a contact between the G81 backbone and R269 side chain in WT β. Taken together, the MD simulations suggest that the changes in specific hydrogen-bond contacts and other noncovalent interactions induced by the point mutations result in significant changes in conformation and dynamics that are consistent with the observed experimental results for both the stabilizing and destabilizing mutations.

Our rational approach resulted in variants with stabilizing and tunable destabilizing mutations that likely render the clamp closed or open, respectively. We also report here MD simulations that rationalize our observations of the effects of these mutations on the biological activities of the resulting clamp variants, as well as the complete hydrogen-bond-interaction map. We are now working to create stable monomers in solution by designing the next generation of mutations.

SUPPORTING MATERIAL

Supporting Material can be found online at https://doi.org/10.1016/j.bpj.2019.06.035.

AUTHOR CONTRIBUTIONS

B.N.K., H.G., A.A.R., F.F.-L., D.M.K., G.A.C., and P.J.B. designed research. B.N.K., H.G., A.A.R., S.L., K.J.D.F., A.C., and M.L.L. performed research and analyzed data. B.N.K., H.G., A.A.R., S.L., K.J.D.F., M.L.L., F.F.-L., D.M.K., G.A.C., and P.J.B. wrote the manuscript.

ACKNOWLEDGMENTS

We thank Jane Compton for technical assistance and Heidi Erlandsen from the UConn Biophysics Core for help with ITC.

This work was supported by the National Institutes of Health (R01GM123239 to P.J.B. and D.M.K. and R01GM108583 to G.A.C.) and the National Science Foundation (MCB-1615946 to P.J.B.; MCB-1615866 to D.M.K.; CHE-1654274 CAREER Award to F.F.-L.). Computing time from UNT CASCaM with support from National Science Foundation CHE-1531468 is gratefully acknowledged.

REFERENCES

1. Georgescu, R. E., S. S. Kim, …, M. O'Donnell. 2008. Structure of a sliding clamp on DNA. *Cell.* 132:43–54.
2. Sutton, M. D. 2010. Coordinating DNA polymerase traffic during high and low fidelity synthesis. *Biochim. Biophys. Acta.* 1804:1167–1179.
3. Bloom, L. B., X. Chen, …, M. F. Goodman. 1997. Fidelity of *Escherichia coli* DNA polymerase III holoenzyme. The effects of beta, gamma complex processivity proteins and epsilon proofreading exonuclease on nucleotide misincorporation efficiencies. *J. Biol. Chem.* 272:27919–27930.
4. Kong, X. P., R. Onrust, …, J. Kuriyan. 1992. Three-dimensional structure of the beta subunit of *E. coli* DNA polymerase III holoenzyme: a sliding DNA clamp. *Cell.* 69:425–437.
5. Krishna, T. S., X. P. Kong, …, J. Kuriyan. 1994. Crystal structure of the eukaryotic DNA polymerase processivity factor PCNA. *Cell.* 79:1233–1243.
6. Williams, G. J., K. Johnson, …, J. H. Naismith. 2006. Structure of the heterotrimeric PCNA from *Sulfolobus solfataricus*. *Acta Crystallogr. Sect. F Struct. Biol. Cryst. Commun.* 62:944–948.
7. Moarefi, I., D. Jeruzalmi, …, J. Kuriyan. 2000. Crystal structure of the DNA polymerase processivity factor of T4 bacteriophage. *J. Mol. Biol.* 296:1215–1223.
8. Oakley, A. J., P. Prosselkov, …, N. E. Dixon. 2003. Flexibility revealed by the 1.85 A crystal structure of the beta sliding-clamp subunit of *Escherichia coli* DNA polymerase III. *Acta Crystallogr. D Biol. Crystallogr.* 59:1192–1199.
9. Gulbis, J. M., Z. Kelman, …, J. Kuriyan. 1996. Structure of the C-terminal region of p21(WAF1/CIP1) complexed with human PCNA. *Cell.* 87:297–306.
10. Wang, K., Z. Shi, …, D. Cheng. 2013. Structure of PCNA from Drosophila melanogaster. *Acta Crystallogr. Sect. F Struct. Biol. Cryst. Commun.* 69:387–392.

11. Matsumiya, S., Y. Ishino, and K. Morikawa. 2001. Crystal structure of an archaeal DNA sliding clamp: proliferating cell nuclear antigen from *Pyrococcus furiosus*. *Protein Sci.* 10:17–23.
12. Fay, P. J., K. O. Johanson, …, R. A. Bambara. 1981. Size classes of products synthesized processively by DNA polymerase III and DNA polymerase III holoenzyme of *Escherichia coli*. *J. Biol. Chem.* 256:976–983.
13. Yao, N. Y., R. E. Georgescu, …, M. E. O'Donnell. 2009. Single-molecule analysis reveals that the lagging strand increases replisome processivity but slows replication fork progression. *Proc. Natl. Acad. Sci. USA.* 106:13236–13241.
14. Maki, H., and A. Kornberg. 1985. The polymerase subunit of DNA polymerase III of *Escherichia coli*. II. Purification of the alpha subunit, devoid of nuclease activities. *J. Biol. Chem.* 260:12987–12992.
15. Maki, S., and A. Kornberg. 1988. DNA polymerase III holoenzyme of *Escherichia coli*. II. A novel complex including the gamma subunit essential for processive synthesis. *J. Biol. Chem.* 263:6555–6560.
16. López de Saro, F. J., and M. O'Donnell. 2001. Interaction of the beta sliding clamp with MutS, ligase, and DNA polymerase I. *Proc. Natl. Acad. Sci. USA.* 98:8376–8380.
17. Hughes, A. J., Jr., S. K. Bryan, …, C. S. McHenry. 1991. *Escherichia coli* DNA polymerase II is stimulated by DNA polymerase III holoenzyme auxiliary subunits. *J. Biol. Chem.* 266:4568–4573.
18. Bonner, C. A., P. T. Stukenberg, …, M. F. Goodman. 1992. Processive DNA synthesis by DNA polymerase II mediated by DNA polymerase III accessory proteins. *J. Biol. Chem.* 267:11431–11438.
19. Dalrymple, B. P., K. Kongsuwan, …, P. A. Jennings. 2001. A universal protein-protein interaction motif in the eubacterial DNA replication and repair systems. *Proc. Natl. Acad. Sci. USA.* 98:11627–11632.
20. Stukenberg, P. T., P. S. Studwell-Vaughan, and M. O'Donnell. 1991. Mechanism of the sliding beta-clamp of DNA polymerase III holoenzyme. *J. Biol. Chem.* 266:11328–11334.
21. Naktinis, V., J. Turner, and M. O'Donnell. 1996. A molecular switch in a replication machine defined by an internal competition for protein rings. *Cell.* 84:137–145.
22. Wagner, J., S. Fujii, …, R. P. Fuchs. 2000. The beta clamp targets DNA polymerase IV to DNA and strongly increases its processivity. *EMBO Rep.* 1:484–488.
23. Lenne-Samuel, N., J. Wagner, …, R. P. Fuchs. 2002. The processivity factor beta controls DNA polymerase IV traffic during spontaneous mutagenesis and translesion synthesis *in vivo*. *EMBO Rep.* 3:45–49.
24. Tang, M., P. Pham, …, M. F. Goodman. 2000. Roles of *E. coli* DNA polymerases IV and V in lesion-targeted and untargeted SOS mutagenesis. *Nature.* 404:1014–1018.
25. Tang, M., X. Shen, …, M. F. Goodman. 1999. UmuD′(2)C is an error-prone DNA polymerase, *Escherichia coli* pol V. *Proc. Natl. Acad. Sci. USA.* 96:8919–8924.
26. Bunting, K. A., S. M. Roe, and L. H. Pearl. 2003. Structural basis for recruitment of translesion DNA polymerase Pol IV/DinB to the beta-clamp. *EMBO J.* 22:5883–5892.
27. Indiani, C., P. McInerney, …, M. O'Donnell. 2005. A sliding-clamp toolbelt binds high- and low-fidelity DNA polymerases simultaneously. *Mol. Cell.* 19:805–815.
28. Kath, J. E., S. Jergic, …, J. J. Loparo. 2014. Polymerase exchange on single DNA molecules reveals processivity clamp control of translesion synthesis. *Proc. Natl. Acad. Sci. USA.* 111:7647–7652.
29. Kath, J. E., S. Chang, …, J. J. Loparo. 2016. Exchange between *Escherichia coli* polymerases II and III on a processivity clamp. *Nucleic Acids Res.* 44:1681–1690.
30. Katayama, T., T. Kubota, …, K. Sekimizu. 1998. The initiator function of DnaA protein is negatively regulated by the sliding clamp of the *E. coli* chromosomal replicase. *Cell.* 94:61–71.
31. Kurz, M., B. Dalrymple, …, K. Kongsuwan. 2004. Interaction of the sliding clamp beta-subunit and Hda, a DnaA-related protein. *J. Bacteriol.* 186:3508–3515.
32. Beyer, A. 1997. Sequence analysis of the AAA protein family. *Protein Sci.* 6:2043–2058.
33. Hedglin, M., R. Kumar, and S. J. Benkovic. 2013. Replication clamps and clamp loaders. *Cold Spring Harb. Perspect. Biol.* 5:a010165.
34. Kelch, B. A. 2016. Review: the lord of the rings: structure and mechanism of the sliding clamp loader. *Biopolymers.* 105:532–546.
35. Kelch, B. A., D. L. Makino, …, J. Kuriyan. 2012. Clamp loader ATPases and the evolution of DNA replication machinery. *BMC Biol.* 10:34.
36. Marzahn, M. R., J. N. Hayner, …, L. B. Bloom. 2014. The ATP sites of AAA+ clamp loaders work together as a switch to assemble clamps on DNA. *J. Biol. Chem.* 289:5537–5548.
37. Goedken, E. R., M. Levitus, …, J. Kuriyan. 2004. Fluorescence measurements on the *E.coli* DNA polymerase clamp loader: implications for conformational changes during ATP and clamp binding. *J. Mol. Biol.* 336:1047–1059.
38. Kazmirski, S. L., M. Podobnik, …, J. Kuriyan. 2004. Structural analysis of the inactive state of the *Escherichia coli* DNA polymerase clamp-loader complex. *Proc. Natl. Acad. Sci. USA.* 101:16750–16755.
39. Paschall, C. O., J. A. Thompson, …, L. B. Bloom. 2011. The *Escherichia coli* clamp loader can actively pry open the β-sliding clamp. *J. Biol. Chem.* 286:42704–42714.
40. Jeruzalmi, D., M. O'Donnell, and J. Kuriyan. 2001. Crystal structure of the processivity clamp loader gamma (gamma) complex of *E. coli* DNA polymerase III. *Cell.* 106:429–441.
41. Simonetta, K. R., S. L. Kazmirski, …, J. Kuriyan. 2009. The mechanism of ATP-dependent primer-template recognition by a clamp loader complex. *Cell.* 137:659–671.
42. Yao, N., J. Turner, …, M. O'Donnell. 1996. Clamp loading, unloading and intrinsic stability of the PCNA, beta and gp45 sliding clamps of human, *E. coli* and T4 replicases. *Genes Cells.* 1:101–113.
43. Soumillion, P., D. J. Sexton, and S. J. Benkovic. 1998. Clamp subunit dissociation dictates bacteriophage T4 DNA polymerase holoenzyme disassembly. *Biochemistry.* 37:1819–1827.
44. Alley, S. C., V. K. Shier, …, S. J. Benkovic. 1999. Sliding clamp of the bacteriophage T4 polymerase has open and closed subunit interfaces in solution. *Biochemistry.* 38:7696–7709.
45. Millar, D., M. A. Trakselis, and S. J. Benkovic. 2004. On the solution structure of the T4 sliding clamp (gp45). *Biochemistry.* 43:12723–12727.
46. Trakselis, M. A., S. C. Alley, …, S. J. Benkovic. 2001. Creating a dynamic picture of the sliding clamp during T4 DNA polymerase holoenzyme assembly by using fluorescence resonance energy transfer. *Proc. Natl. Acad. Sci. USA.* 98:8368–8375.
47. Gadkari, V. V., S. R. Harvey, …, Z. Suo. 2018. Investigation of sliding DNA clamp dynamics by single-molecule fluorescence, mass spectrometry and structure-based modeling. *Nucleic Acids Res.* 46:3103–3118.
48. De Biasio, A., R. Sánchez, …, F. J. Blanco. 2011. Reduced stability and increased dynamics in the human proliferating cell nuclear antigen (PCNA) relative to the yeast homolog. *PLoS One.* 6:e16600.
49. Chen, S., M. K. Levin, …, M. M. Hingorani. 2009. Mechanism of ATP-driven PCNA clamp loading by *S. cerevisiae* RFC. *J. Mol. Biol.* 388:431–442.
50. Thompson, J. A., M. R. Marzahn, …, L. B. Bloom. 2012. Replication factor C is a more effective proliferating cell nuclear antigen (PCNA) opener than the checkpoint clamp loader, Rad24-RFC. *J. Biol. Chem.* 287:2203–2209.
51. Sakato, M., Y. Zhou, and M. M. Hingorani. 2012. ATP binding and hydrolysis-driven rate-determining events in the RFC-catalyzed PCNA clamp loading reaction. *J. Mol. Biol.* 416:176–191.
52. Binder, J. K., L. G. Douma, …, M. Levitus. 2014. Intrinsic stability and oligomerization dynamics of DNA processivity clamps. *Nucleic Acids Res.* 42:6476–6486.
53. Tainer, J. A., J. A. McCammon, and I. Ivanov. 2010. Recognition of the ring-opened state of proliferating cell nuclear antigen by replication

factor C promotes eukaryotic clamp-loading. *J. Am. Chem. Soc.* 132:7372–7378.

54. Purohit, A., J. K. England, …, M. Levitus. 2017. Electrostatic interactions at the dimer interface stabilize the *E. coli* β sliding clamp. *Biophys. J.* 113:794–804.
55. Fang, J., J. R. Engen, and P. J. Beuning. 2011. *Escherichia coli* processivity clamp β from DNA polymerase III is dynamic in solution. *Biochemistry.* 50:5958–5968.
56. Fang, J., P. Nevin, …, P. J. Beuning. 2014. Conformational analysis of processivity clamps in solution demonstrates that tertiary structure does not correlate with protein dynamics. *Structure.* 22:572–581.
57. Jeruzalmi, D., O. Yurieva, …, J. Kuriyan. 2001. Mechanism of processivity clamp opening by the delta subunit wrench of the clamp loader complex of *E. coli* DNA polymerase III. *Cell.* 106:417–428.
58. Oakley, A. J. 2016. Dynamics of open DNA sliding clamps. *PLoS One.* 11:e0154899.
59. Leu, F. P., M. M. Hingorani, …, M. O'Donnell. 2000. The delta subunit of DNA polymerase III holoenzyme serves as a sliding clamp unloader in *Escherichia coli*. *J. Biol. Chem.* 275:34609–34618.
60. Alyami, E. M., A. A. Rizzo, …, D. M. Korzhnev. 2017. NMR resonance assignments for the N-terminal domain of the δ subunit of the *E. coli* γ clamp loader complex. *Biomol. NMR Assign.* 11:169–173.
61. Erster, O., and M. Liscovitch. 2010. A modified inverse PCR procedure for insertion, deletion, or replacement of a DNA fragment in a target sequence and its application in the ligand interaction scan method for generation of ligand-regulated proteins. *Methods Mol. Biol.* 634: 157–174.
62. Heltzel, J. M., S. K. Scouten Ponticelli, …, M. D. Sutton. 2009. Sliding clamp-DNA interactions are required for viability and contribute to DNA polymerase management in *Escherichia coli*. *J. Mol. Biol.* 387:74–91.
63. Bianco, P. R., S. Pottinger, …, U. Varshney. 2017. The IDL of *E. coli* SSB links ssDNA and protein binding by mediating protein-protein interactions. *Protein Sci.* 26:227–241.
64. Yu, C., H. Y. Tan, …, P. R. Bianco. 2016. SSB binds to the RecG and PriA helicases *in vivo* in the absence of DNA. *Genes Cells.* 21:163–184.
65. Ericsson, U. B., B. M. Hallberg, …, P. Nordlund. 2006. Thermofluor-based high-throughput stability optimization of proteins for structural studies. *Anal. Biochem.* 357:289–298.
66. Fernandez-Lima, F., D. A. Kaplan, …, M. A. Park. 2011. Gas-phase separation using a trapped ion mobility spectrometer. *Int. J. Ion Mobil. Spectrom.* 14:93–98.
67. Fernandez-Lima, F. A., D. A. Kaplan, and M. A. Park. 2011. Note: integration of trapped ion mobility spectrometry with mass spectrometry. *Rev. Sci. Instrum.* 82:126106.
68. McDaniel, E. W., and E. A. Mason. 1973. Mobility and Diffusion of Ions in Gases. John Wiley and Sons, Inc, New York.
69. Hernandez, D. R., J. D. Debord, …, F. Fernandez-Lima. 2014. Ion dynamics in a trapped ion mobility spectrometer. *Analyst (Lond.).* 139:1913–1921.
70. Sutton, M. D., J. M. Duzen, and R. W. Maul. 2005. Mutant forms of the *Escherichia coli* beta sliding clamp that distinguish between its roles in replication and DNA polymerase V-dependent translesion DNA synthesis. *Mol. Microbiol.* 55:1751–1766.
71. Sambrook, J., E. F. Fritsch, and T. Maniatis. 1989. Molecular Cloning: A Laboratory Manual. Cold Spring Harbor Laboratory Press, Cold Spring Harbor, NY.
72. Parasuram, R., T. A. Coulther, …, P. J. Beuning. 2018. Prediction of active site and distal residues in *E. coli* DNA polymerase III alpha polymerase activity. *Biochemistry.* 57:1063–1072.
73. Case, D. A., D. S. Cerutti, …, P. A. Kollman. 2017. AMBER 2017. University of California, San Francisco, CA.
74. Maier, J. A., C. Martinez, …, C. Simmerling. 2015. ff14SB: improving the accuracy of protein side chain and backbone parameters from ff99SB. *J. Chem. Theory Comput.* 11:3696–3713.
75. Götz, A. W., M. J. Williamson, …, R. C. Walker. 2012. Routine microsecond molecular dynamics simulations with AMBER on GPUs. 1. generalized born. *J. Chem. Theory Comput.* 8:1542–1555.
76. Le Grand, S., A. W. Gotz, and R. C. Walker. 2013. SPFP: speed without compromise-a mixed precision model for GPU accelerated molecular dynamics simulations. *Comput. Phys. Commun.* 184:374–380.
77. Berendsen, H. J. C., J. P. M. Postma, …, J. R. Haak. 1984. Molecular dynamics with coupling to an external bath. *J. Chem. Phys.* 81:3684–3690.
78. Essmann, U., L. Perera, …, L. G. Pedersen. 1995. A smooth particle mesh Ewald method. *J. Chem. Phys.* 103:8577–8593.
79. Roe, D. R., and T. E. Cheatham, III. 2013. PTRAJ and CPPTRAJ: software for processing and analysis of molecular dynamics trajectory data. *J. Chem. Theory Comput.* 9:3084–3095.
80. Humphrey, W., A. Dalke, and K. Schulten. 1996. VMD: visual molecular dynamics. *J. Mol. Graph.* 14:33–38, 27–38.
81. ChemAxon 2017. MarvinSketch v17.26.0. http://www.chemaxon.com.
82. Stewart, J., M. M. Hingorani, …, M. O'Donnell. 2001. Mechanism of beta clamp opening by the delta subunit of *Escherichia coli* DNA polymerase III holoenzyme. *J. Biol. Chem.* 276:19182–19189.
83. Bertram, J. G., L. B. Bloom, …, M. F. Goodman. 1998. Pre-steady state analysis of the assembly of wild type and mutant circular clamps of *Escherichia coli* DNA polymerase III onto DNA. *J. Biol. Chem.* 273:24564–24574.
84. Simonetta, K. R. 2010. Structural studies of the mechanism of clamp loading by clamp loader complexes, in molecular and cell biology, PhD thesis (University of California).
85. Beuning, P. J., D. Sawicka, …, G. C. Walker. 2006. Two processivity clamp interactions differentially alter the dual activities of UmuC. *Mol. Microbiol.* 59:460–474.
86. Heltzel, J. M., R. W. Maul, …, M. D. Sutton. 2009. A model for DNA polymerase switching involving a single cleft and the rim of the sliding clamp. *Proc. Natl. Acad. Sci. USA.* 106:12664–12669.
87. Scouten Ponticelli, S. K., J. M. Duzen, and M. D. Sutton. 2009. Contributions of the individual hydrophobic clefts of the *Escherichia coli* beta sliding clamp to clamp loading, DNA replication and clamp recycling. *Nucleic Acids Res.* 37:2796–2809.
88. Park, M. S., and M. O'Donnell. 2009. The clamp loader assembles the beta clamp onto either a 3′ or 5′ primer terminus: the underlying basis favoring 3′ loading. *J. Biol. Chem.* 284:31473–31483.
89. Kelch, B. A., D. L. Makino, …, J. Kuriyan. 2011. How a DNA polymerase clamp loader opens a sliding clamp. *Science.* 334:1675–1680.
90. Bowman, G. D., M. O'Donnell, and J. Kuriyan. 2004. Structural analysis of a eukaryotic sliding DNA clamp-clamp loader complex. *Nature.* 429:724–730.
91. Naktinis, V., R. Onrust, …, M. O'Donnell. 1995. Assembly of a chromosomal replication machine: two DNA polymerases, a clamp loader, and sliding clamps in one holoenzyme particle. II. Intermediate complex between the clamp loader and its clamp. *J. Biol. Chem.* 270:13358–13365.
92. Burnouf, D. Y., V. Olieric, …, P. Dumas. 2004. Structural and biochemical analysis of sliding clamp/ligand interactions suggest a competition between replicative and translesion DNA polymerases. *J. Mol. Biol.* 335:1187–1197.

Biophysical Journal, Volume *117*

Supplemental Information

Dynamics of the *E. coli* β-Clamp Dimer Interface and Its Influence on DNA Loading

Bilyana N. Koleva, Hatice Gokcan, Alessandro A. Rizzo, Socheata Lim, Kevin Jeanne Dit Fouque, Angelina Choy, Melissa L. Liriano, Francisco Fernandez-Lima, Dmitry M. Korzhnev, G. Andrés Cisneros, and Penny J. Beuning

Supporting Methods and Results

Protein Expression and Purification

For most experiments, *E. coli* BL21(DE3) was transformed with pET11T expressing WT β or β clamp variants. Transformants were selected on Luria-Bertani (LB) plates supplemented with ampicillin. A 50-mL starter culture in a shake flask (200 rpm) was grown overnight at 37 °C. A 1-L culture was seeded for each protein and grown at 37 °C until an optical density (OD) at 600 nm of 1.0 was reached. Protein expression was induced with isopropyl β-D-1-thiogalactopyranoside (IPTG) to a final concentration of 1 mM at 22 °C for 16-18 h. Cells were harvested by centrifugation for 10 min at 6,750 × g at 4 °C and frozen at -80 °C or lysed immediately. Protein overexpression was confirmed using sodium dodecyl sulfate-polyacrylamide gel electrophoresis (SDS-PAGE).

Cell pellets for β clamp purification were resuspended on ice in 20 mM HEPES, pH 7.5, 100 mM NaCl, 0.1 mM EDTA, 2 mM DTT, 10% glycerol (Buffer A) supplemented with 10 μg/mL phenylmethanesulfonyl fluoride (PMSF), and cOmplete^{TM} mini protease inhibitor cocktail (Roche, Sigma, St. Louis, MO). Cells were lysed by sonication and cell debris was pelleted by centrifugation at 14,000 × g at 4 °C for 1 h. The lysate was loaded onto a 2 × 5 mL HiTrap DEAE FF (GE Healthcare) column and eluted with Buffer A and increasing NaCl concentration to 1 M. Pooled fractions were diluted 1:1 in a buffer containing 20 mM HEPES, pH 7.5, 0.1 mM EDTA, 2 mM DTT, 10% glycerol, and 1 M ammonium sulfate, loaded onto 2 × 5 mL HiTrap Phenyl FF high sub (GE Healthcare), and eluted in a buffer with the same composition except ammonium sulfate was omitted. Pooled fractions were concentrated using VivaSpin 20, 10,000 Da MWCO concentrators (Sartorius, Cambridge, MA) and loaded onto Superdex 75 (GE Healthcare). Proteins were stored in 20 mM HEPES, pH 7.5, 50 mM NaCl, 0.1 mM EDTA, 1 mM DTT, and 10% glycerol at -80 °C for subsequent analysis. Protein concentration was measured using the Bradford assay with bovine serum albumin (BSA) as a reference (Sigma). Final purity was assessed using SDS-PAGE.

For ITC, *E. coli* BL21(DE3) was transformed with plasmids encoding corresponding proteins and grown to mid-log phase at 37 °C in LB media containing 50 μg/mL kanamycin. Protein expression was induced by 1 mM IPTG at 20 °C overnight. Cells were harvested and lysed by sonication. The lysate was centrifuged and filtered, followed by protein purification on a Talon Co^{2+} affinity column (Clontech, Mountain View, CA). The His-tag was cleaved with thrombin and a final purification step was performed on HiLoad Superdex-75 (mini-δ) or Superdex-200 (β clamp) size-exclusion columns (GE Healthcare). The purified mini-δ and β clamp variants were concentrated to 0.6-0.7 mM and 0.1 mM, respectively, and dialyzed into a buffer containing 100 mM sodium phosphate, 100 mM NaCl, 500 μM β-mercaptoethanol (βME), pH 7.4. Prior to ITC studies, protein samples were cleared by centrifugation at 14,000 rpm for 30 min and degassed for at least 30 min.

ATPase assay

The assay was performed as per the BIOMOL® Green manual (Enzo Life Sciences). To anneal DNA, equimolar amounts of 5'-biotinylated primer (5′-Biotin-AGTTCTTCTGCAATAACTGGCCGT CGTTTGAAGATTTCG-3′, IDT, Coralville, IA) and 5′-biotinylated template (5′-biotin-CCATTCTGT AACGCCAGGGTTTTCGCAGTCAACATTCGAAATCTTCAAACGACGGCCAGTTATTGC-3′) were combined in STE buffer (10 mM Tris-HCl, pH 8.0, 50 mM NaCl, 0.1 mM EDTA). Annealing reactions were incubated at 95 °C for 2 min, 50 °C for 30 min, and slowly cooled to room temperature. Assay samples were prepared in 100 μL reactions containing 50 pmol β_2, 50 pmol γ complex, 50 pmol annealed dsDNA, and 1 mM ATP in 1x ATPase assay buffer (30 mM HEPES, pH 7.5, 1 mM DTT, 7 mM $MgCl_2$).

Reactions were incubated for 5 min at 37 °C, following which 1 mL of BIOMOL® Green reagent was added to each sample and incubated for an additional 20 min at 22 °C. Samples (1 mL) were then transferred to a cuvette and OD_{620} was measured. For quantitation, a standard curve was prepared using inorganic phosphate. The linear range of the assay in the cuvette format is from 0.5 nmol to 16 nmol of phosphate released. Each reaction was assembled in triplicate. Average nmol of phosphate released and standard deviations are reported.

Clamp loading assay

To anneal DNA, equimolar amounts of 5′-biotinylated primer (5′-AGTTCTTCTGC AATAACTGGCCGTCGTTTGAAGATTTCG-3′) and template (5′-ACGACCGTCCCATTCTGTAACG CCAGGGTTTTCGCAGTCAACATTCGAAATCTTCAAACGACGGCCAGTTATTGC-3′) were added in STE buffer (10 mM Tris-HCl, pH 8.0, 50 mM NaCl, 0.1 mM EDTA). Annealing reactions were incubated at 95 °C for 2 min, 50 °C for 30 min, and slowly cooled to room temperature. Streptavidin magnetic beads (New England Biolabs) were washed with 1x B/W buffer (5 mM Tris-HCl, pH 7.5, 0.5 mM EDTA, 1 M NaCl) three times to remove storage solution. For the bioconjugation, 200 pmol of biotinylated dsDNA was combined with 1 mg of streptavidin beads in 40 µL in 1x B/W buffer. Binding was achieved by incubation at 22 °C for 1 h on a rotator. The beads were washed two times in 1x B/W buffer to remove unbound DNA and two more times in 1x loading assay buffer (30 mM HEPES, pH 7.5, 7 mM $MgSO_4$, 1 mM DTT, 1 mM CHAPS). Loading reactions were performed by resuspending the bead-DNA conjugate in 25 µL 1x loading assay buffer containing 200 pmol β_2, 200 pmol γ complex, 1 mM ATP, and 5 µg SSB. After 5 min incubation at 37 °C, 5 µL bead resuspension was applied to the magnet, with the unloaded β in the supernatant and the loaded β in the pellet fraction. The beads were washed three times in 1x loading assay buffer by tapping gently to remove unbound proteins. At indicated time points (0, 60 min), 10 µL bead resuspension was removed from the reaction and applied to the magnet to probe for loaded vs. unloaded β. The reactions were incubated at 22 °C on a rotator while collecting the time points. Loading controls were assembled separately to show the amount of β in reactions. All samples were normalized based on the quantified amount of protein in the loading control and incubated in 1x SDS loading buffer (62.5 mM Tris-HCl, pH 6.8, 0.01% Bromophenol Blue, 2.5% βME, 10% glycerol, 2% SDS) for 10 min at 95 °C prior to resolution by 12% SDS-PAGE. Assays were carried out with loading amounts within the linear range of quantitation, or if samples were diluted prior to loading in order to remain within the linear range, this dilution factor was accounted for in the calculations of the amount of β in each fraction. Electrophoresed proteins were transferred to polyvinylidene difluoride (PVDF) membrane in 10 mM CAPS, pH 10.0, 10% methanol buffer. Gels were stained with Coomassie gel stain after transfer to ensure proteins were transferred. Membranes were blocked overnight in 2.5% milk/2.5% BSA in 20 mM Tris-HCl, pH 7.6, 137 mM NaCl, 0.1% Tween-20 (TBS-T). Membranes were incubated with rabbit anti-β primary antibody and goat anti-rabbit Alexa-647 (Thermo Fisher) secondary antibody for 1 h each at 22 °C in 2.5% milk/2.5% BSA TBS-T buffer. Membranes were washed three times, 5 min each in TBS-T buffer after each antibody incubation. Proteins were detected on a Storm 860 phosphorimager using excitation at 635 nm and analyzed using ImageQuant TL 1D Gel Analysis software (GE Healthcare). Loading assays were repeated three times and the average amount of loaded/unloaded β and the standard deviations are reported.

Immunoblotting

Wild-type β and variants of the β clamp were expressed in MS120 cells at the non-permissive growth temperature 37 °C. Expression was induced with 0.5 mM IPTG in LB for 18 h. The OD_{600} was measured and used to normalize the volume of cells to be collected for each variant. Centrifugation was used to harvest cells that were then resuspended in 300 µL 0.85% saline and 100 µL 4X SDS-dye. Samples were

heated to 95 °C for 30 min to lyse the cells and denature the proteins. Proteins were resolved by 16% SDS-PAGE and transferred to polyvinylidene difluoride (PVDF) membranes at 4 °C and processed as above. Membranes were then imaged on an iBright (Invitrogen) on the Alex-fluor 647 channel.

Molecular Dynamics Results

Effect of the mutations on atomic fluctuations. Nine residues with a change in relative RMSF value greater than ±1 Å were observed for the different variants (Fig. S11). P20′, L21′, and G22′ on Monomer B become more mobile in the L82E variant (Fig. S11, *green*) relative to WT β. D120′, which is located on the inter-domain connector loop (IDCL) between Domain 1 and Domain 2, becomes more mobile in the S107R variant (Fig. S11, *cyan*), while the mobility of D120′ is observed to be either very similar to that of the WT protein or calculated to be less than that of WT β for all other variants. The mobility of G209, G210, and D211 are affected by different mutations, where the highest increase is seen for the T45R variant (Fig. S11, *yellow*). The same region on Monomer B (G209′, G210′, and D211′) becomes less mobile in the context of almost all of the mutations except for the T47R variant (Fig. S11, *magenta*). L248, which is in close proximity to the hydrophobic pocket where β-interacting proteins bind (residues 247, 360, 363) (19, 57, 89), becomes more mobile on Monomer A in the β L82E I272A variant (Fig. S11, *blue*). Similar results are seen for the residue K250, located on the IDCL between Domain 2 and Domain 3.

Cross correlation in the dimer interface. Helix-3 (H3) and Helix-21 (H21) are observed to be mostly positively correlated in the L82E, T45R, and S107R variants (Fig. S12A, region colors: *blue-cyan*) while negative correlations are found for the remaining systems relative to WT β. Most of the residues on H3 and Sheet-5A (S5A) are computed as negatively correlated in the L82D variant (Fig. S12A, region colors: *blue-yellow*) while H3 and Sheet-6A (S6A) are found positively correlated in the T45R variant (Fig. S12A, region colors: *blue-orange*). The L82D variant results in anti-correlation between the tail residues of Sheet-3A (S3A) and H21 unlike in other systems (Fig. S12A, region colors: *red-cyan*). A similar result is found for the correlation between the head residues of Sheet-4A (S4A) and tail residues of H21 in the L82D variant (Fig. S12A, region colors: *green-cyan*). The β L82E variant also exhibited increased correlation between the tail residues of S4A and H21 (Fig. S12A, region colors: *green-cyan*), while the additional I272A mutation in the L82E I272A variant results in the highest S4A-H21 correlations.

In the case of the second domain interface between Domain 3 and Domain 1′, Helix-10 (H10) and Helix-14 (H14) are observed to be correlated in the T45R and S107R variants (Fig. S12B, region colors: *blue-cyan*). Almost all the residues on H10 are positively correlated with Sheet-5D (S5D) (Fig. S12B, region colors: *blue-yellow*) and Sheet-6D (S6D) (Fig. S12B, region colors: *blue-orange*) in the T45R variant. Almost all residues on H14 are negatively correlated with Sheet-3D (S3D) and Sheet-4D in the L82E variant but the additional I272A and I272′A mutations in the L82E I272A variant result in positive correlations between H14 and S4D in this variant.

The mutations in the L82E and L82E I272A variants increase the number of residues in β sheets that are correlated with each other on the domain interface between Domain 1 and Domain 3′. The region composed of residues from L82 to R96 in particular is found to be highly correlated with the region composed of residues Y282′ to N295′ in these variants. It is noteworthy that the magnitude of the correlations between these β sheets is the highest in the L82E I272A variant relative to the other systems. The loops comprising residues 82-86 and 274′-279′ in the L82D variant have the highest anti-correlation for the Domain 1:Domain 3′ interface (Fig. S12A). For the complementary interface Domain 3:Domain 1′, the corresponding loops (82′-86′ and 274-279) show the highest negative correlations with each other in the L82E variant (Fig. S12B). The loop containing residues 274-279 forms one of the interaction sites with δ (57). In general, the largest perturbations relative to WT β are found in the β L82D, L82E, and L82E I272A variants.

REFERENCES

19. Dalrymple, B.P., K. Kongsuwan, G. Wijffels, N.E. Dixon, and P.A. Jennings 2001. A universal protein-protein interaction motif in the eubacterial DNA replication and repair systems. *Proc Natl Acad Sci U S A*. 98:11627-11632.

57. Jeruzalmi, D., O. Yurieva, Y. Zhao, M. Young, J. Stewart, M. Hingorani, M. O'Donnell, and J. Kuriyan 2001. Mechanism of processivity clamp opening by the delta subunit wrench of the clamp loader complex of *E. coli* DNA polymerase III. *Cell*. 106:417-428.

89. Kelch, B.A., D.L. Makino, M. O'Donnell, and J. Kuriyan 2011. How a DNA polymerase clamp loader opens a sliding clamp. *Science*. 334:1675-1680.

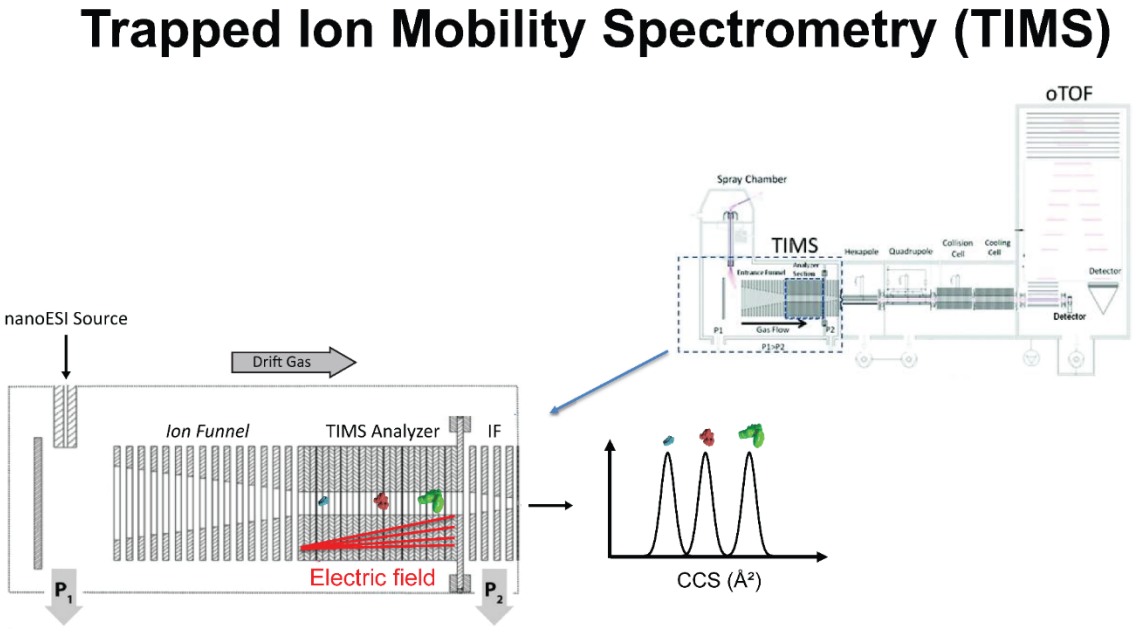

Figure S1. TIMS-MS instrument showing the TIMS cell schematic and TIMS operation.

Table S1. Summary of TIMS experimental ion-neutral collision cross sections (CCS, Å²) and ratios for the multiply protonated species of the *n*-mers clamp variants.

Peptides	CCS (Å²), std. error of mean: ± 0.04%			*n*-mers ratio
	Monomers	Dimers	Tetramers	
Clamp WT	-	**5310** ($[2M+16H]^{16+}$) **5332** ($[2M+17H]^{17+}$) **5325** ($[2M+18H]^{18+}$) **5348** ($[2M+19H]^{19+}$) **5380** ($[2M+20H]^{20+}$)	**7592** ($[4M+25H]^{25+}$) **7682** ($[4M+26H]^{26+}$) **7740** ($[4M+27H]^{27+}$) **7815** ($[4M+28H]^{28+}$)	0/6/1
Clamp L82E	-	**5059** ($[2M+16H]^{16+}$) **5084** ($[2M+17H]^{17+}$) **5129** ($[2M+18H]^{18+}$) **5166** ($[2M+19H]^{19+}$) **5204** ($[2M+20H]^{20+}$)	**7288** ($[4M+24H]^{24+}$) **7341** ($[4M+25H]^{25+}$) **7404** ($[4M+26H]^{26+}$) **7462** ($[4M+27H]^{27+}$) **7537** ($[4M+28H]^{28+}$)	0/3/1
Clamp L82E I272A	**2987** ($[M+10H]^{10+}$) **3066** ($[M+11H]^{11+}$) **3141** ($[M+12H]^{12+}$)	**5063** ($[2M+16H]^{16+}$) **5096** ($[2M+17H]^{17+}$) **5141** ($[2M+18H]^{18+}$) **5173** ($[2M+19H]^{19+}$)	-	1/1/0
Clamp L82D	**2992** ($[M+10H]^{10+}$) **3069** ($[M+11H]^{11+}$) **3144** ($[M+12H]^{12+}$)	-	-	1/0/0

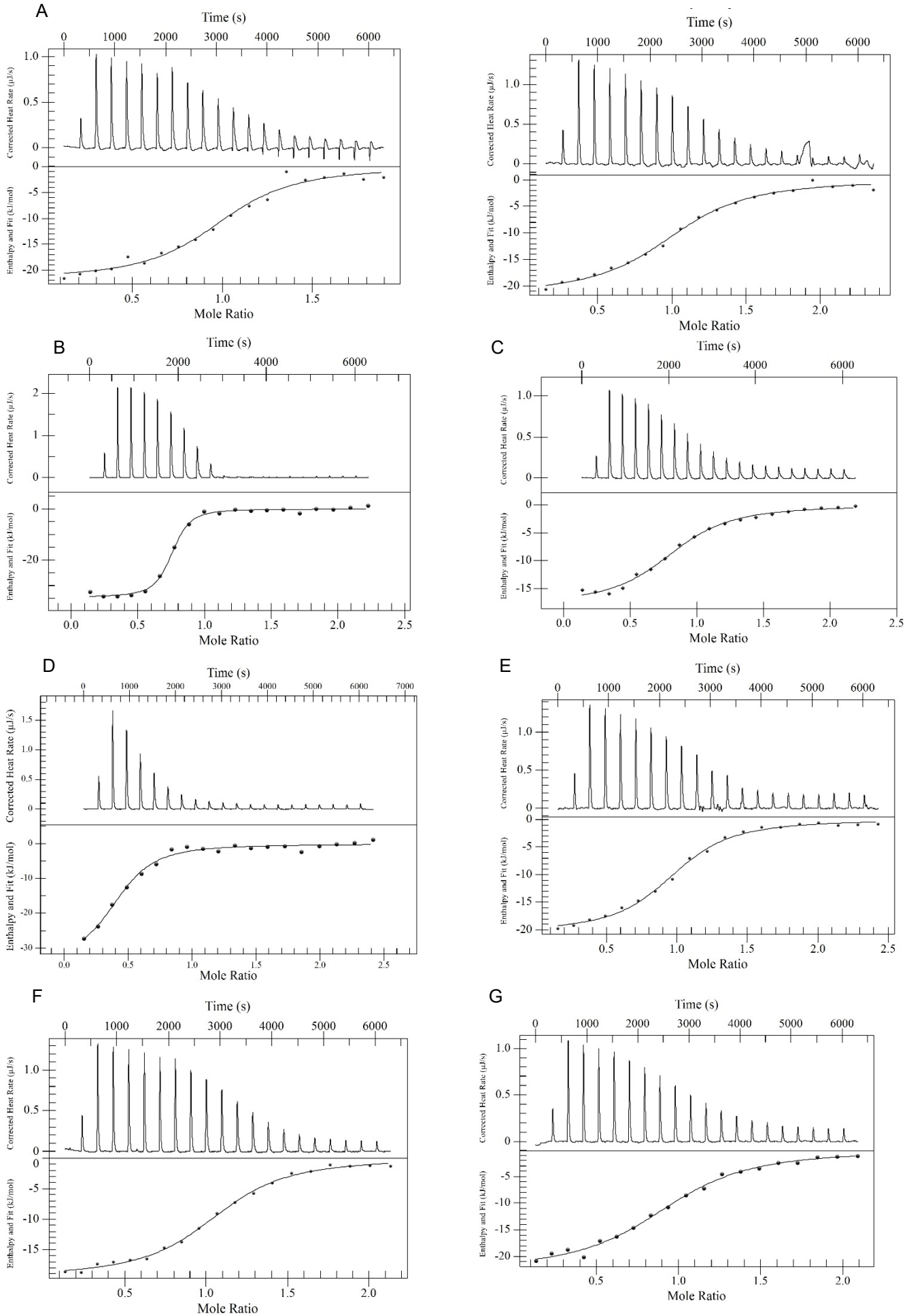
A
Time (s)
Corrected Heat Rate (µJ/s)
Enthalpy and Fit (kJ/mol)
Mole Ratio
B
Time (s)
Corrected Heat Rate (µJ/s)
Enthalpy and Fit (kJ/mol)
Mole Ratio
C
Time (s)
Corrected Heat Rate (µJ/s)
Enthalpy and Fit (kJ/mol)
Mole Ratio
D
Time (s)
Corrected Heat Rate (µJ/s)
Enthalpy and Fit (kJ/mol)
Mole Ratio
E
Time (s)
Corrected Heat Rate (µJ/s)
Enthalpy and Fit (kJ/mol)
Mole Ratio
F
Time (s)
Corrected Heat Rate (µJ/s)
Enthalpy and Fit (kJ/mol)
Mole Ratio
G
Time (s)
Corrected Heat Rate (µJ/s)
Enthalpy and Fit (kJ/mol)
Mole Ratio

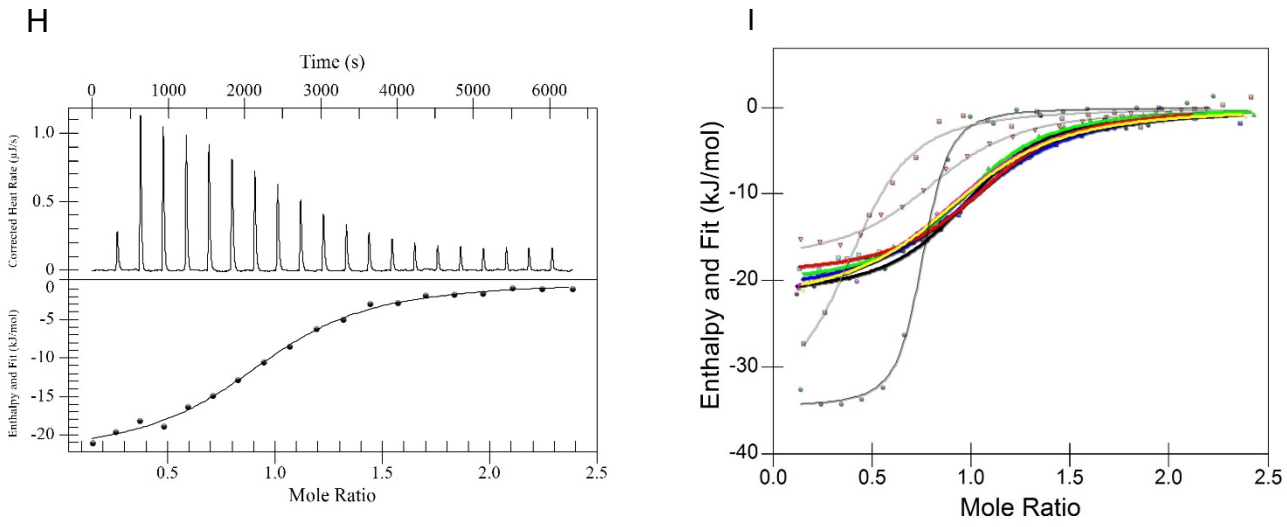

Figure S2. Raw ITC data (top) and integrated heat changes (bottom) obtained during titration into mini-δ solution of the β-clamp variants shown in Table 1: WT (A; 2 replicates), I272A/L273A (B), L82E (C), L82E/I272A (D), S107R (E), S109R (F), T45R (G), T47R (H). (I) Integrated heat changes and their best fits obtained from ITC measurements for mini-δ and β-clamp variants: WT (black, cyan; 2 replicates), I272A L273A (thin black, green circles), S107R (green), S109R (red), T45R (yellow), T47R (magenta), L82E (gray, open triangles), L82E I272A (gray, pink boxes). Thermodynamic parameters are reported in Table 1.

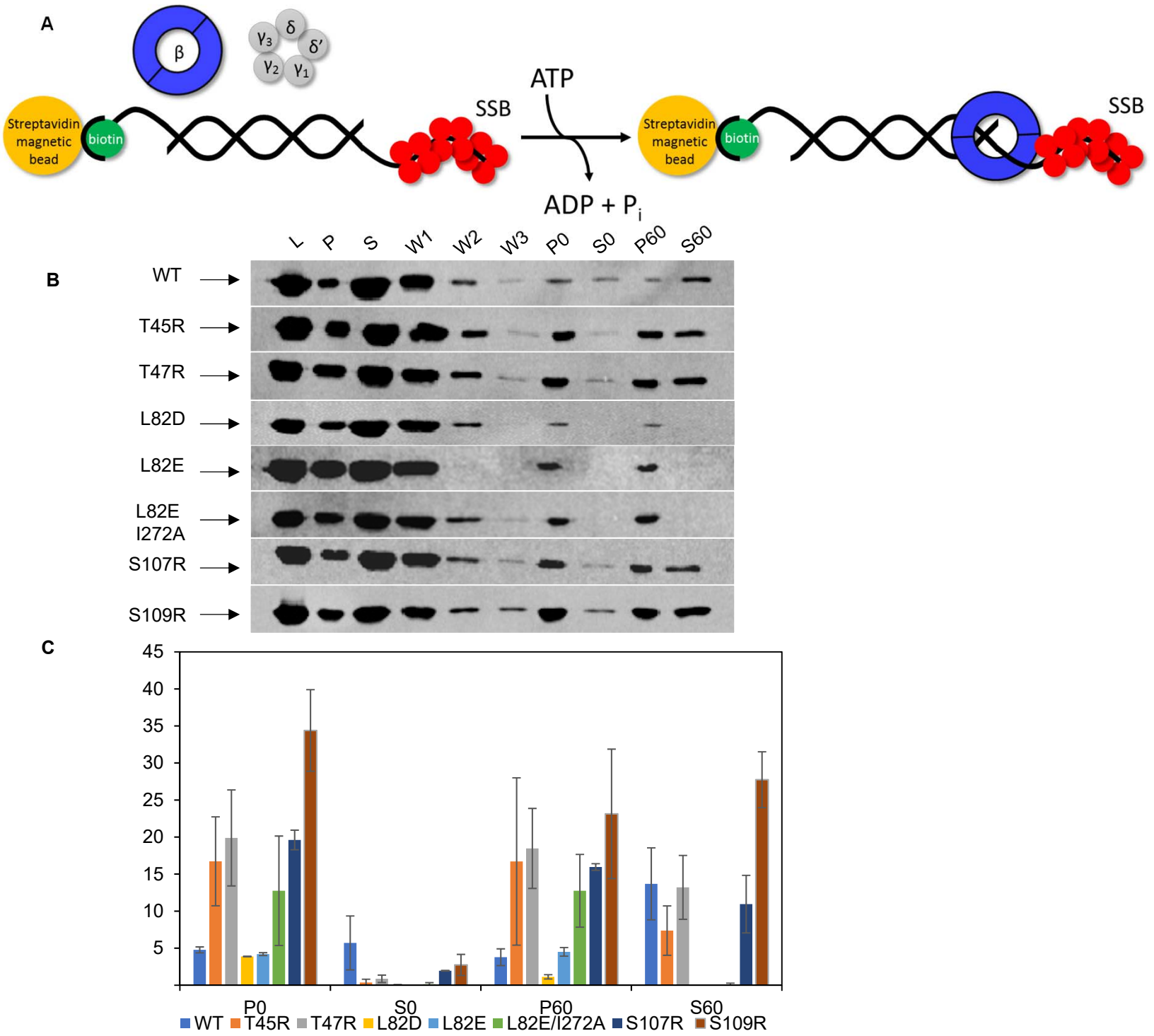

Figure S3. Immunoblot detection of β loaded onto a primer-template substrate using a bead-based assay. (A) Schematic depicting loading of the β clamp onto a primer-template. The biotinylated primer is annealed to a template, resulting in a 3' recessed end. The annealed dsDNA is immobilized on streptavidin magnetic beads. The free 5' end is blocked by SSB (red). Clamp loading reactions are carried out by adding β, γ complex, and ATP to the immobilized DNA at 37 °C. ATP hydrolysis ejects the clamp loader resulting in a stably-loaded clamp. (B) Representative anti-β immunoblots for WT and variant β clamps. Input loading control (L) indicates the amount of β in each loading reaction. Pellet (P) fractions indicate loaded β and supernatant (S) fractions indicate unloaded β. Three consecutive wash steps were performed (shown as W1, W2, and W3). After the wash steps, the pellet and supernatant fractions show the amount of loaded and unloaded β, respectively, for both 0- and 60-min time points. The samples in the first three lanes were diluted 1:4 in order to fit in the linear range of quantitation. In those lanes, the amount loaded/unloaded was multiplied by the dilution factor. (C) Bar graph representing the normalized (based on the input loading control) amount of loaded (pellet) and unloaded (supernatant) β at 0 and 60 min for WT (blue), T45R (orange), T47R (gray), L82D (yellow), L82E (light blue/cyan), L82E I272A (green), S107R (dark blue), and S109R (dark red/brown). Because SSB is present in our reactions and could interact with the β clamp, we investigated whether β interacts with SSB directly by co-expressing and co-purifying both proteins in *E. coli* (Fig. S4).

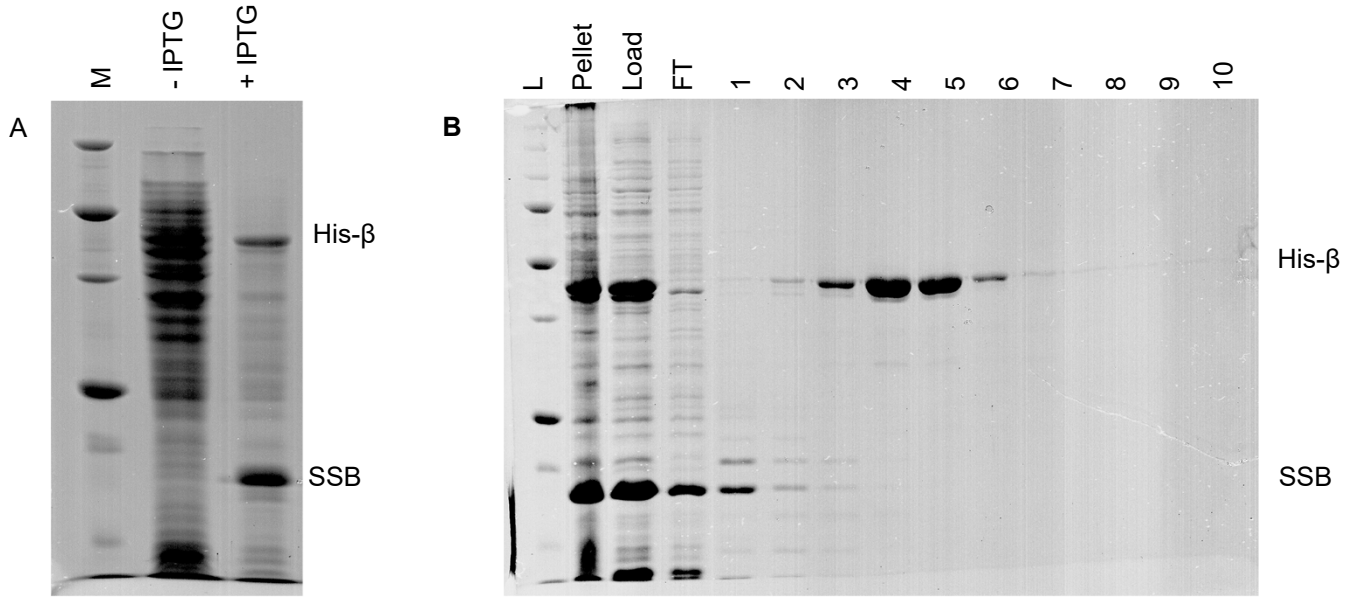

Figure S4. Coexpression to probe for β and SSB interactions. A, Denaturing PAGE showing coexpression of wild-type β (His-tagged) and SSB (untagged). B, Denaturing PAGE demonstrating through Ni^{2+}-affinity chromatography that β and SSB do not coelute. Lysis conditions in the presence and absence of added DNA, additional wash steps and extended gradients were used but it did not appear that β and SSB coelute.

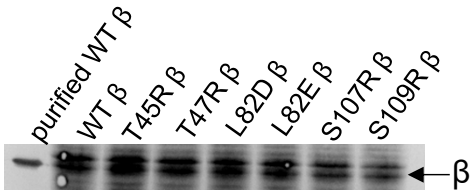

Figure S5. Immunoblot showing expression of WT β and β variants in the MS120 strain at the non-permissive temperature 37 °C. Purified WT β is included as a control. Variants are indicated above the lanes. The L82E I272A does not support growth at 37 °C and therefore was not analyzed.

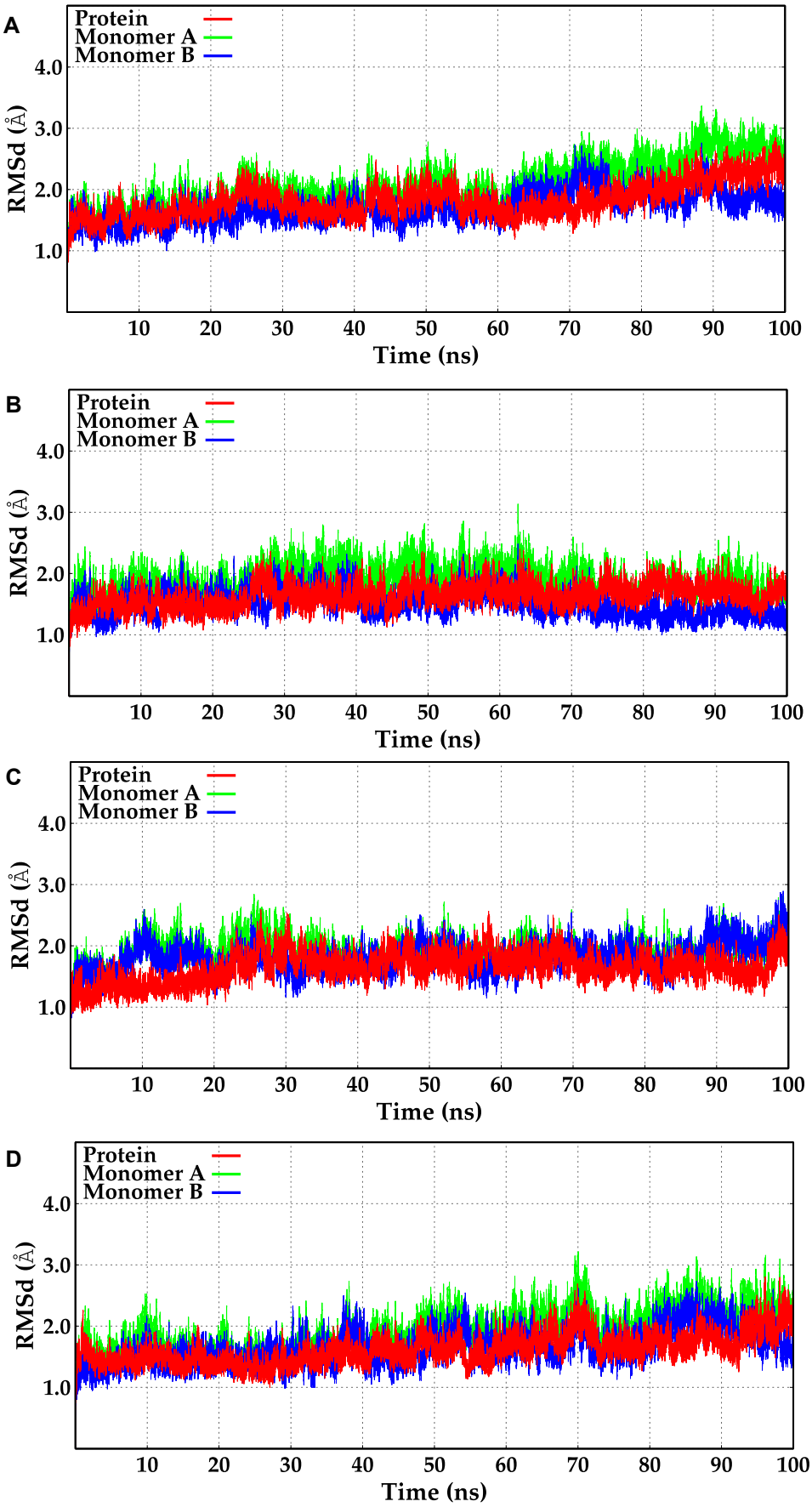

Figure S6. RMSd of backbone atoms (C,C_α,N) along the simulation of (A) WT protein, (B) L82D variant, (C) L82E variant, and (D) L82E I272A variant.

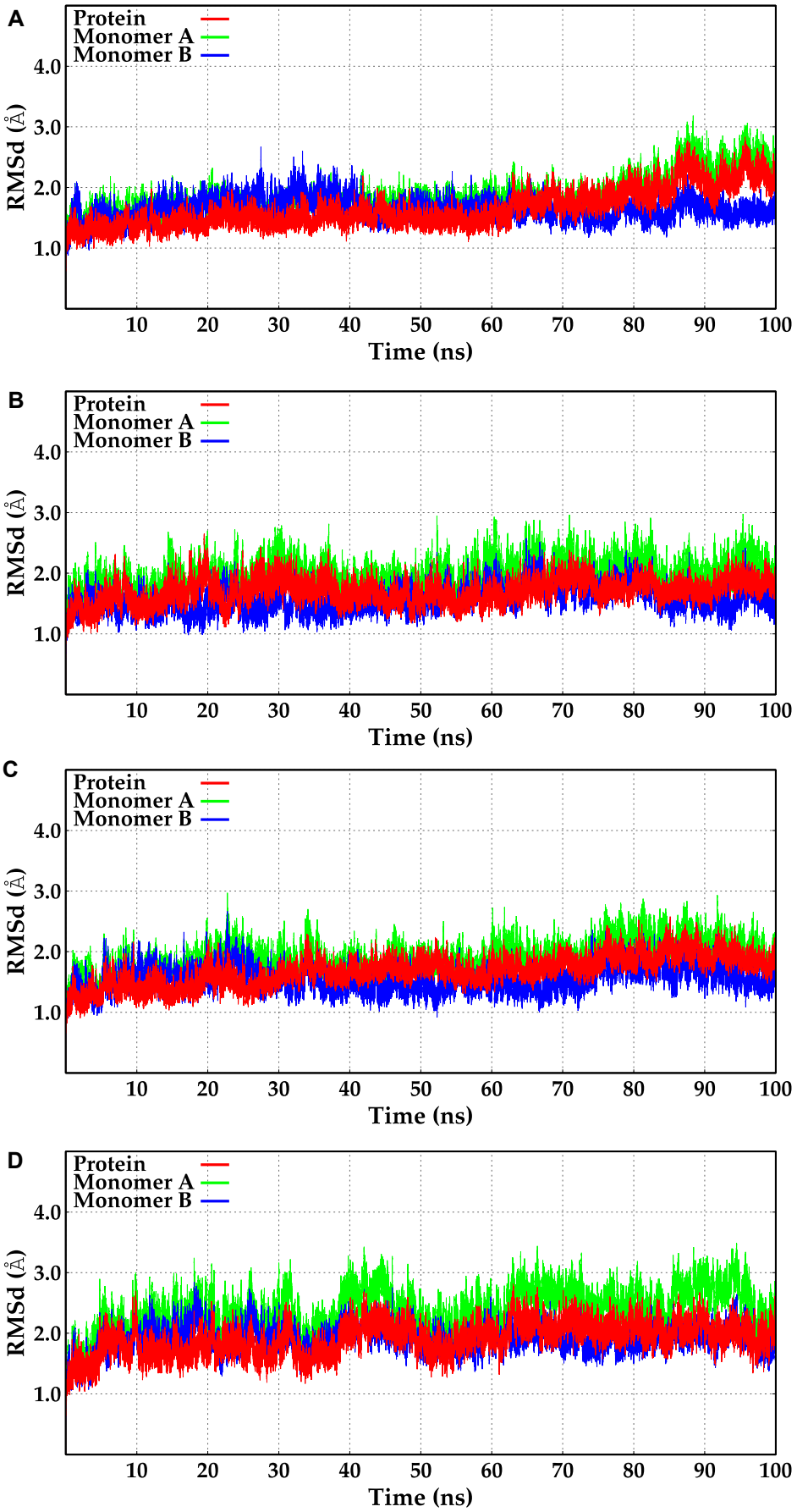

Figure S7. RMSd of backbone atoms (C,C_α,N) along the simulation of (A) T45R variant, (B) T47R variant, (C) S107R variant, and (D) S109R variant.

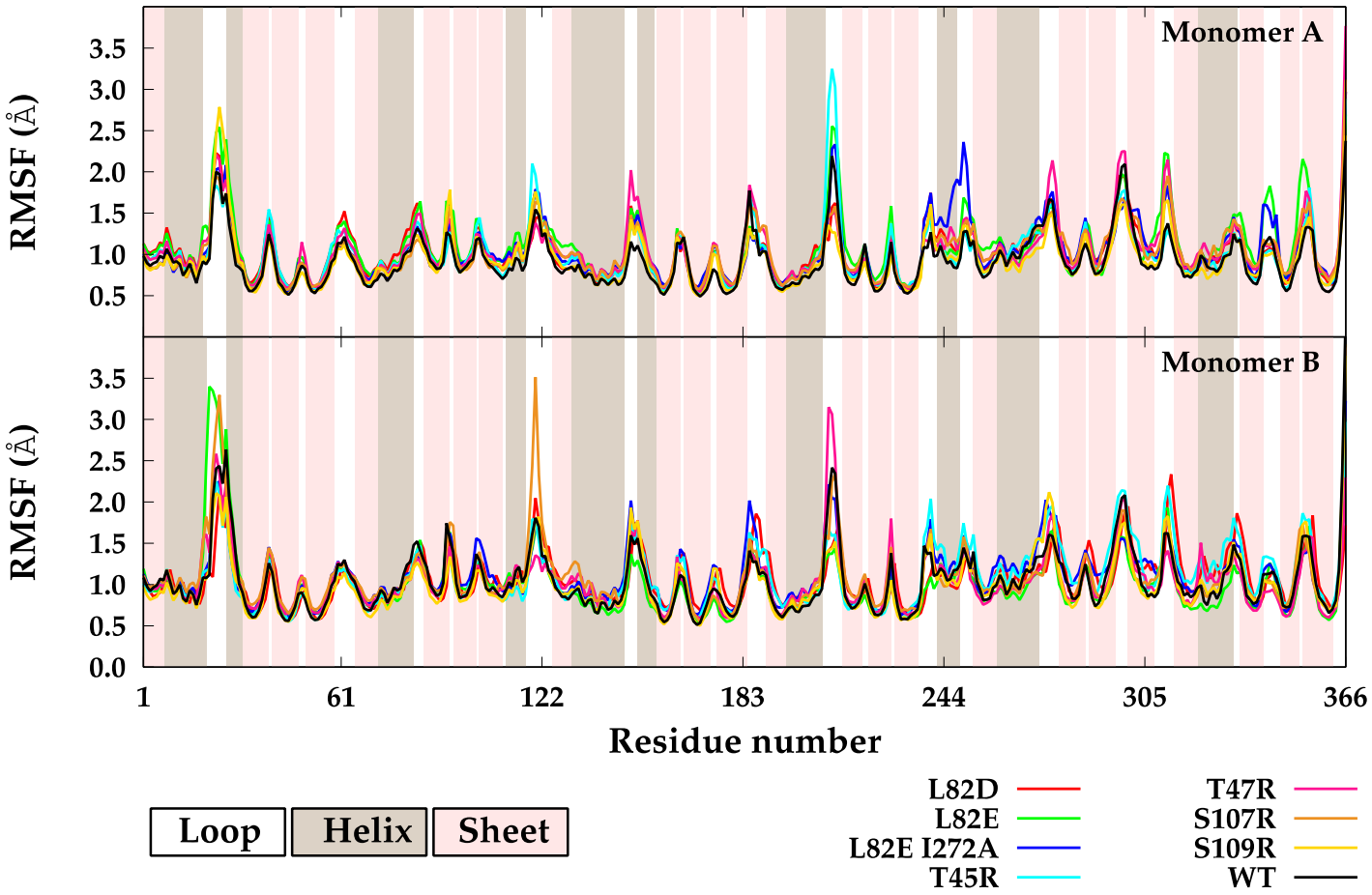

Figure S8. RMSF of residues on Monomer A (top) and Monomer B (bottom) of WT protein (black), L82D variant (red), L82E variant (green), L82E I272A variant (blue), T45R variant (cyan), T47R variant (magenta), S107R variant (orange), and S109R variant (yellow). Residues that are on sheets are represented with light magenta, and the residues that are on helices are represented with light brown columns.

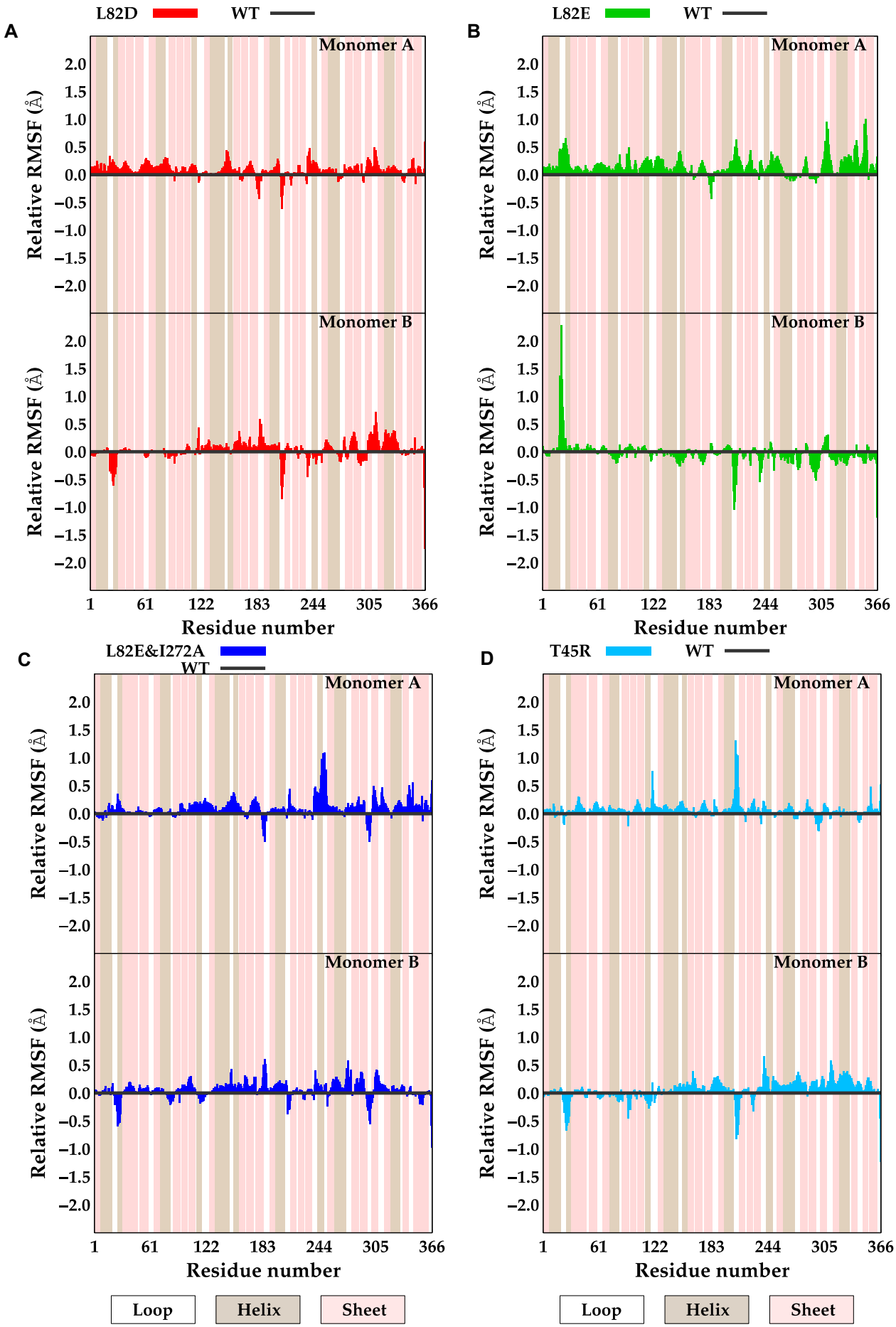

Figure S9. Deviation of the RMSF (Å) values per residue of (A) L82D variant, (B) L82E variant, (C) L82E I272A variant, and (D) T45R variant relative to the WT protein. The relative RMSF values of residues on Monomer A are depicted on top, while the relative RMSF values of residues on Monomer B are depicted on bottom. Residues that are on sheets are represented with light magenta, and the residues that are on helices are represented with light brown columns.

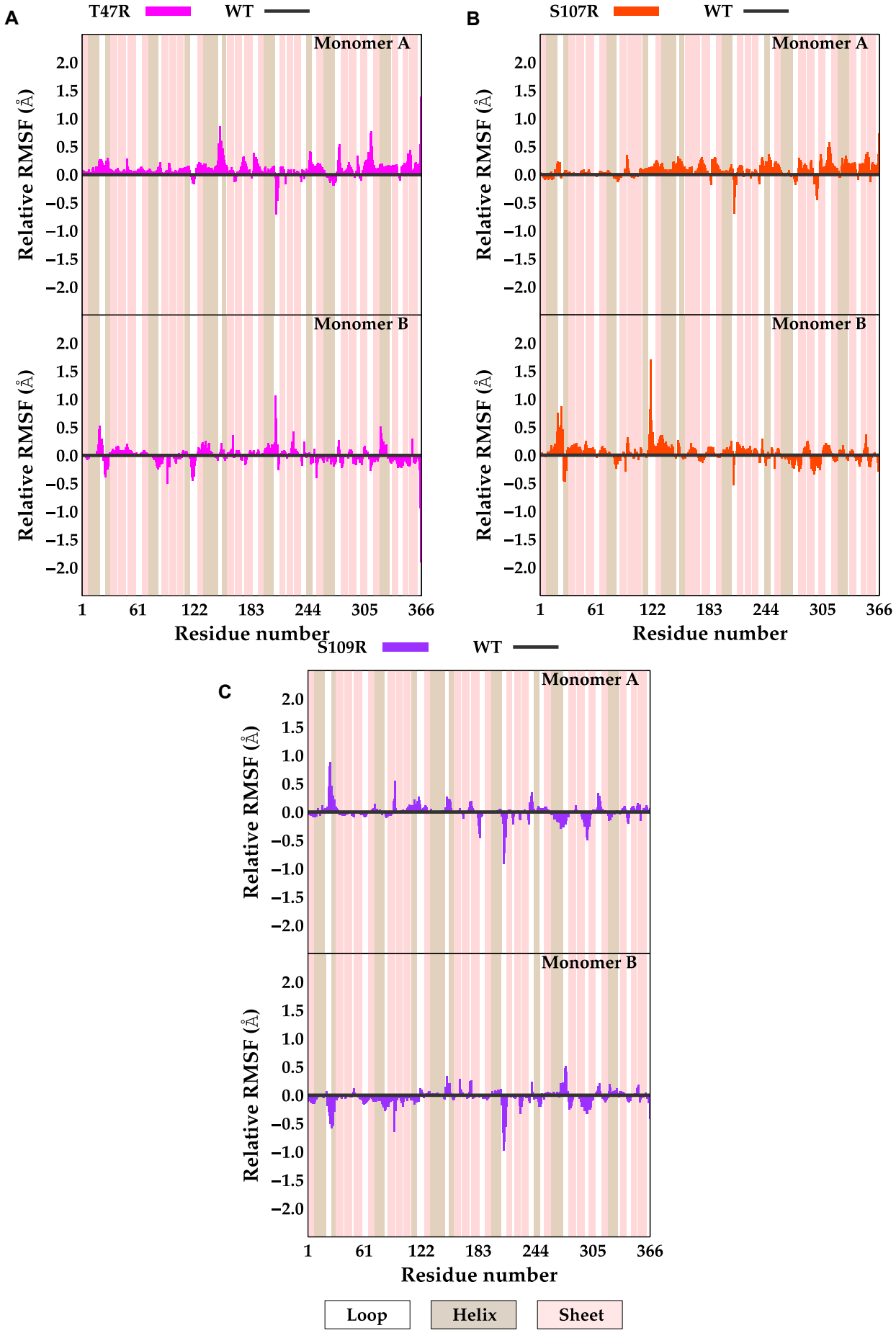

Figure S10. Deviation of the RMSF (Å) values per residue of (A) T47R variant, (B) S107R variant, and (C) S109R variant relative to the WT protein. The relative RMSF values of residues on Monomer A are depicted on top, while the relative RMSF values of residues on Monomer B are depicted on bottom. Residues that are on sheets are represented with light magenta, and the residues that are on helices are represented with light brown columns.

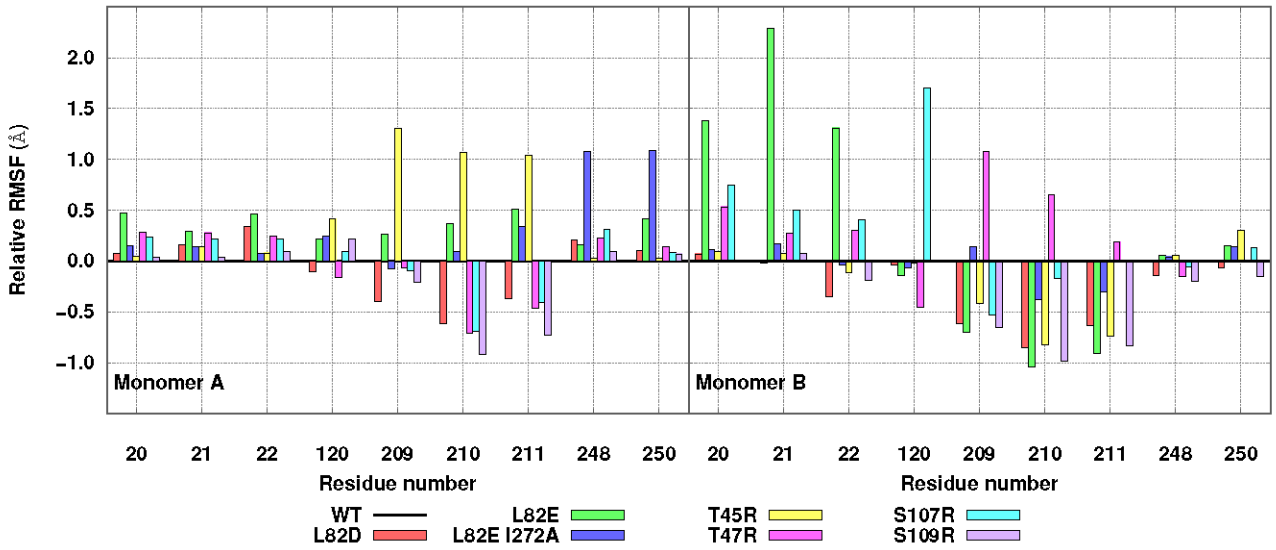

Figure S11. The residues with relative RMSF change greater than 1 Å in at least one monomer. The results for Monomer A are given on the left, and the result for Monomer B are given on the right.

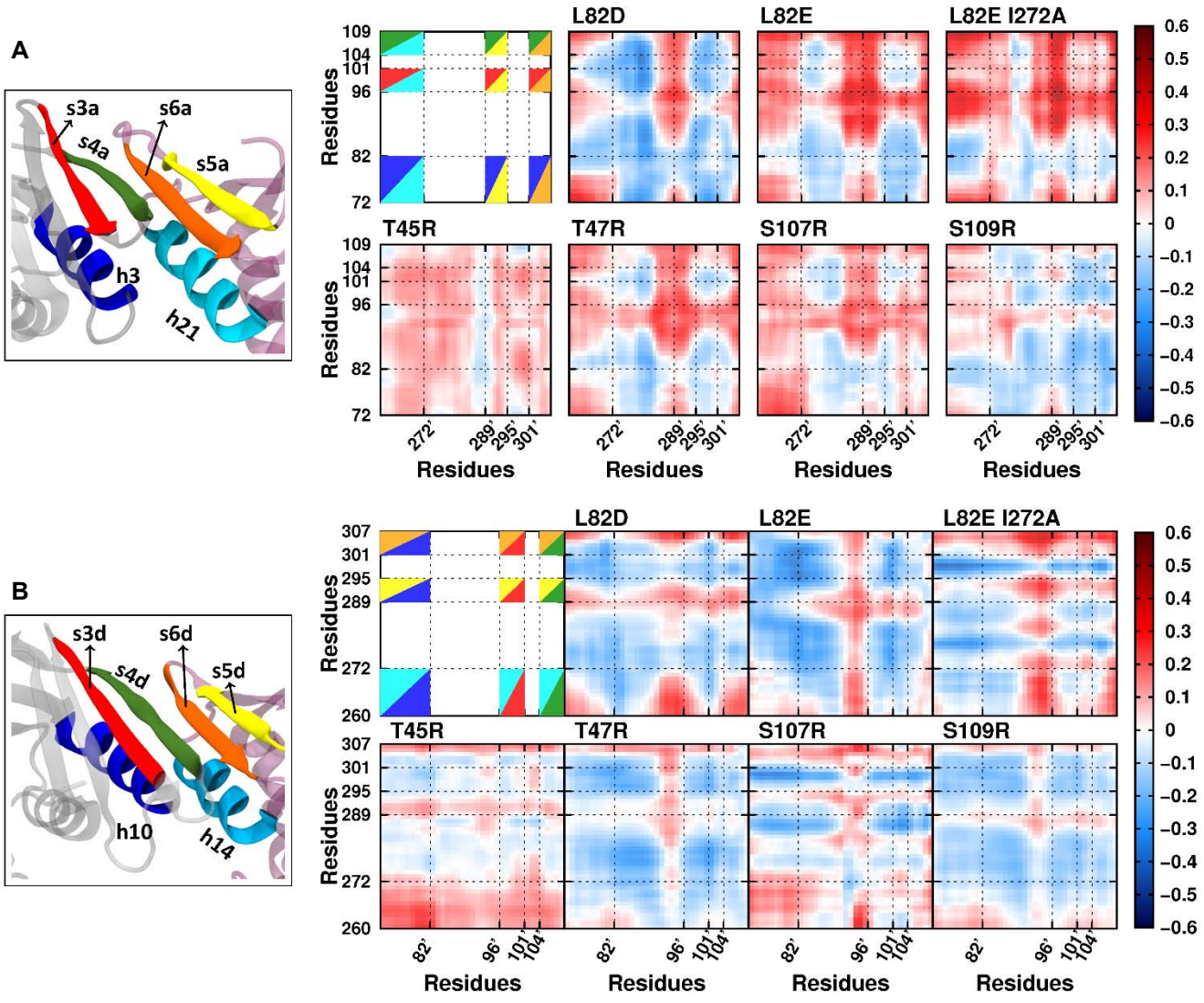

Figure S12. The deviation of the dynamic cross correlations between the residues located on the dimer interfaces of the variants relative to the WT protein. The relative cross correlation between the residues at the (A) dimer interface between Domain 1 and Domain 3', and (B) dimer interface between Domain 3 and Domain 1'. The secondary structures of the residues located at the dimer interfaces are shown on the left in which each secondary structure is depicted with different colors for the corresponding interface. The locations of these secondary structures on the cross-correlation matrices are depicted by the corresponding colors.

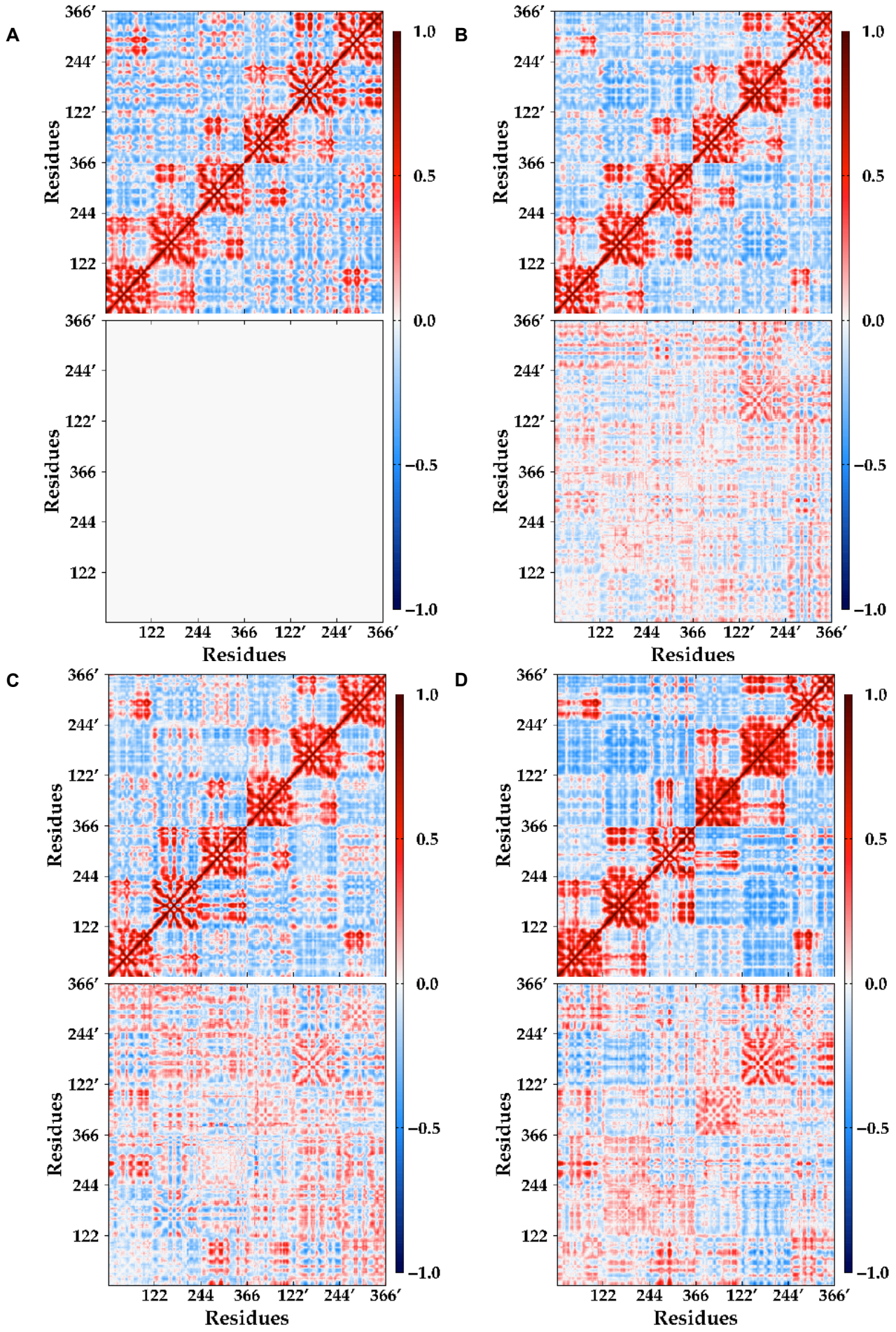

Figure S13. Dynamic cross correlation of the residues of (A) WT protein, (B) L82D variant, (C) L82E variant, and (D) L82E I272A variant. The correlations of the residues are depicted at the top while the deviation of the correlations relative to the reference (WT protein) are given at the bottom.

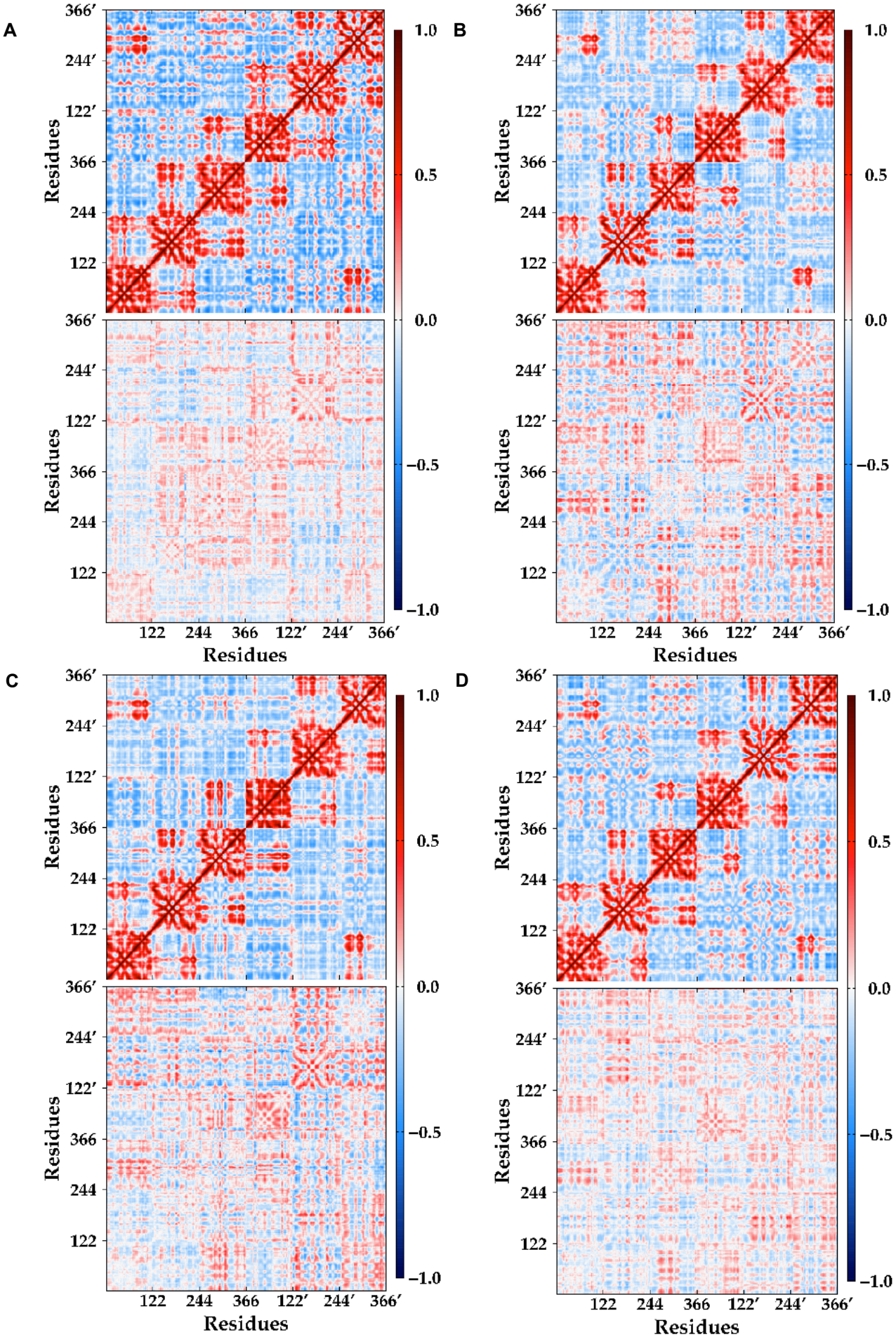

Figure S14. Dynamic cross correlation of the residues of (A) T45R variant, (B) T47R variant, (C) S107R variant, and (D) S109R variant. The correlations of the residues are depicted at the top while the deviation of the correlations relative to the reference (WT protein) are given at the bottom.

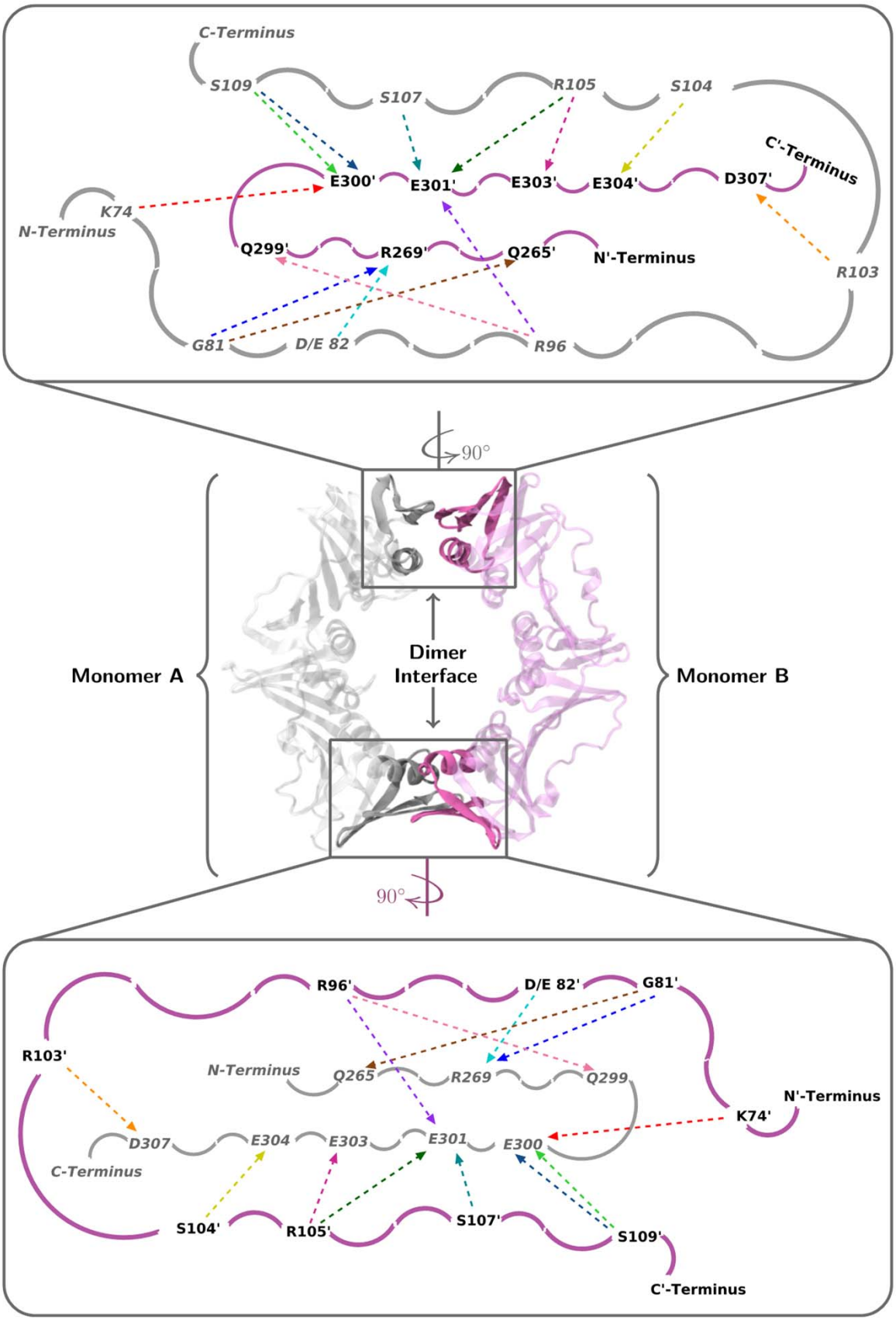

Figure S15. Schematic representation of the hydrogen bond interactions within the dimer interfaces and their locations on the protein. Each of the hydrogen bonds is depicted with a different color. The residues on Monomer A are depicted in gray, while the residues on Monomer B in purple.

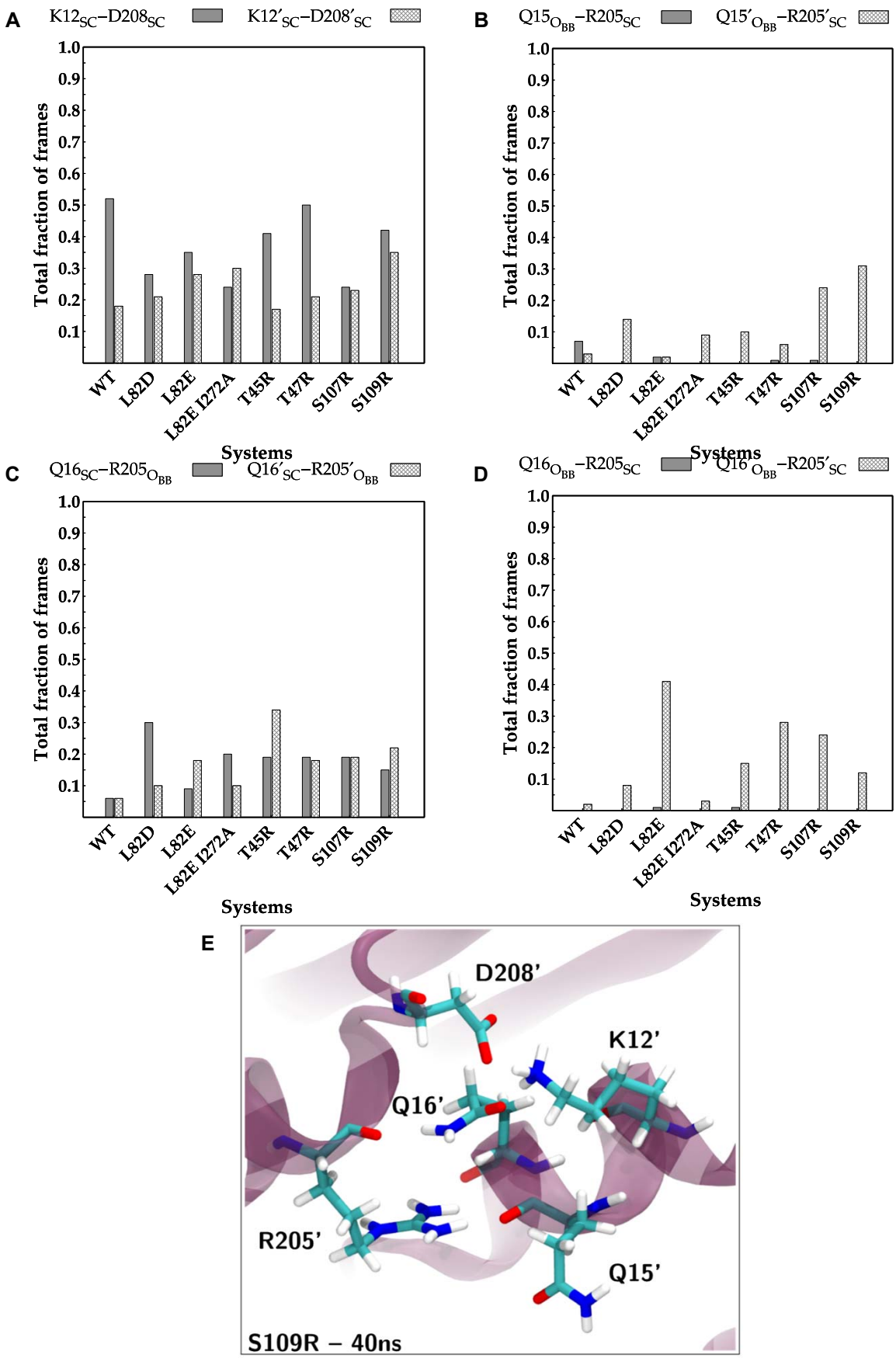

Figure S16. Total fraction of the frames that a hydrogen bond exists between (A) the sidechains of K12 and D208 (solid), and the sidechains of K12' and D208' (pattern fill); (B) the backbone of Q15 and side chain of R205 (solid), and the backbone of Q15' and side chain of R205' (pattern fill); (C) the sidechain of Q16 and backbone of R205 (solid), and the sidechain of Q16' and backbone of R205' (pattern fill); (D) the backbone of Q16 and side chain of R205 (solid), and the backbone of Q16' and side chain of R205' (pattern fill). (E) The three-dimensional representation of the depicted interactions obtained from the trajectory of S109R variant at 40 ns. Sidechains are depicted with subscript "SC" while the backbone Oxygen atoms are depicted with subscript "O_{BB}."

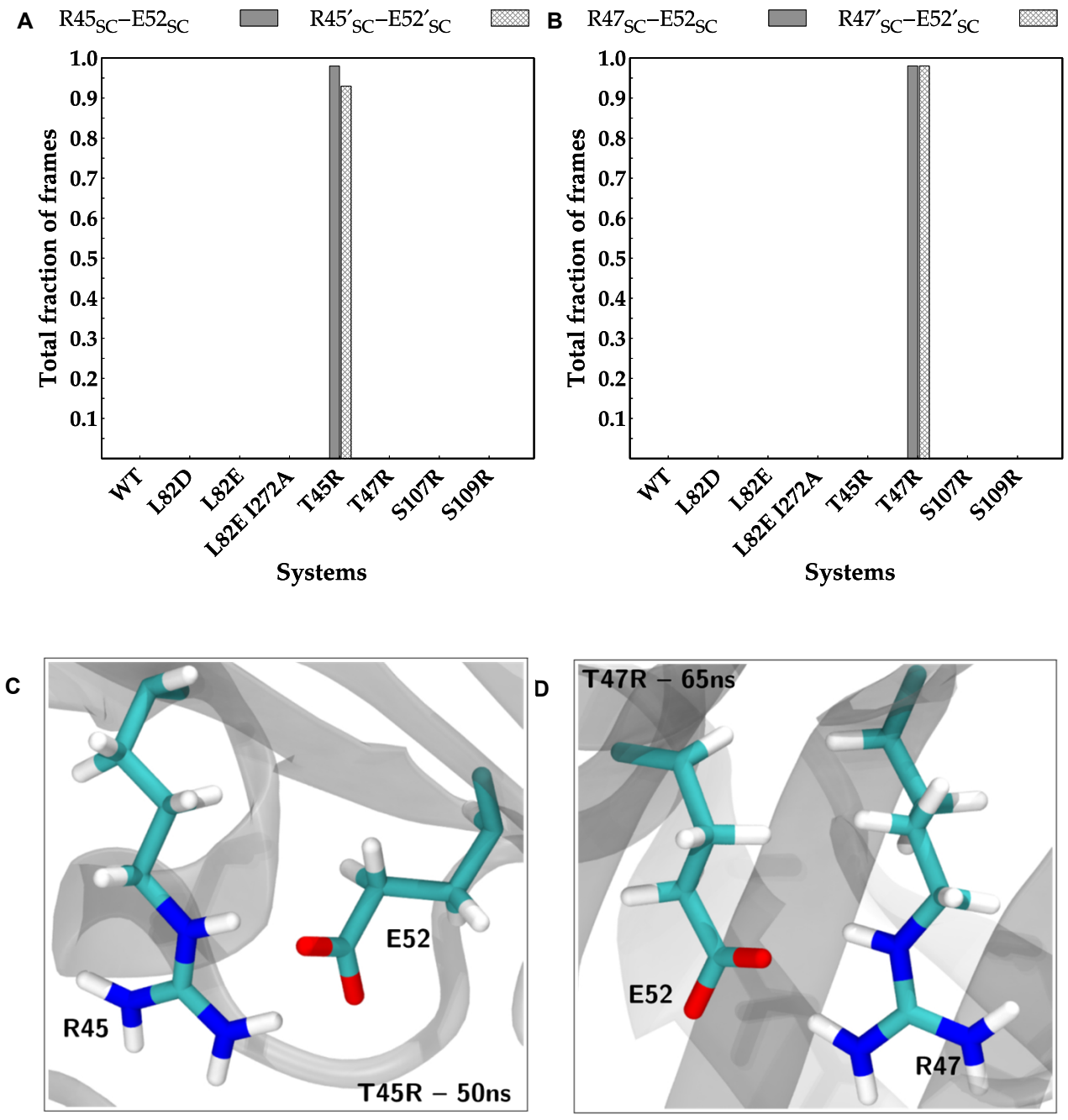

Figure S17. Total fraction of the frames that a hydrogen bond exists between (A) the sidechains of R45 and E52 (solid), and the sidechains of R45' and E52' (pattern fill); (B) the sidechains of R47 and E52 (solid), and the sidechains of R47' and E52' (pattern fill). (C) The three-dimensional representation of the depicted interaction obtained from the trajectory of T45R variant at 50 ns. (D) The three-dimensional representation of the depicted interaction obtained from the trajectory of T47R variant at 65 ns. Sidechains are depicted with subscript "SC."

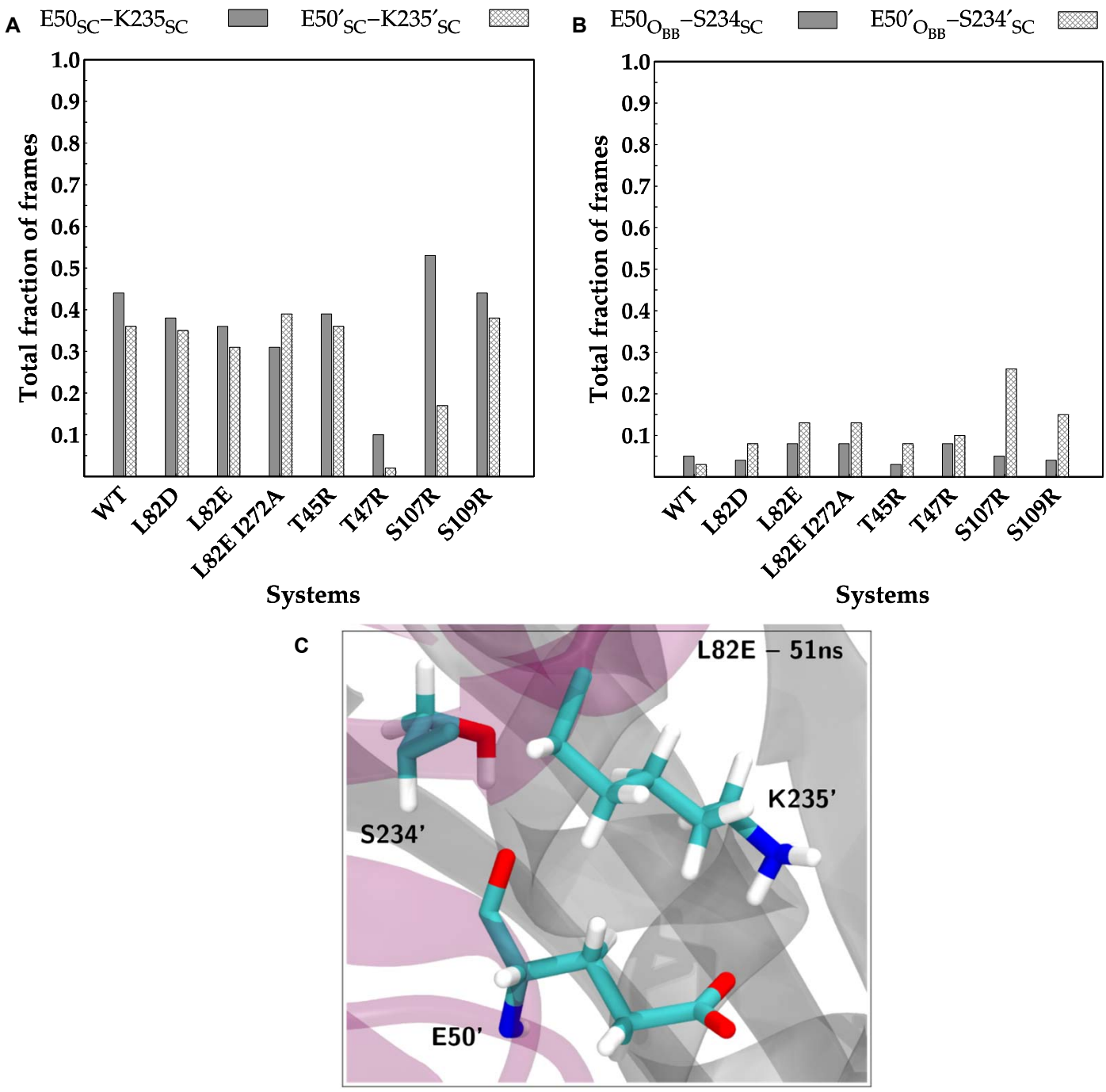

Figure S18. Total fraction of the frames that a hydrogen bond exists between (A) the sidechains of E50 and K235 (solid), and sidechains of E50' and K235' (pattern fill); (B) the backbone of E50 and the sidechain S234 (solid), and the backbone of E50' and the sidechain S234' (pattern fill). (C) The three-dimensional representation of the depicted interaction obtained from the trajectory of L82 variant at 51 ns. Sidechains are depicted with subscript "SC" while the backbone Oxygen atoms are depicted with subscript "O_{BB}."

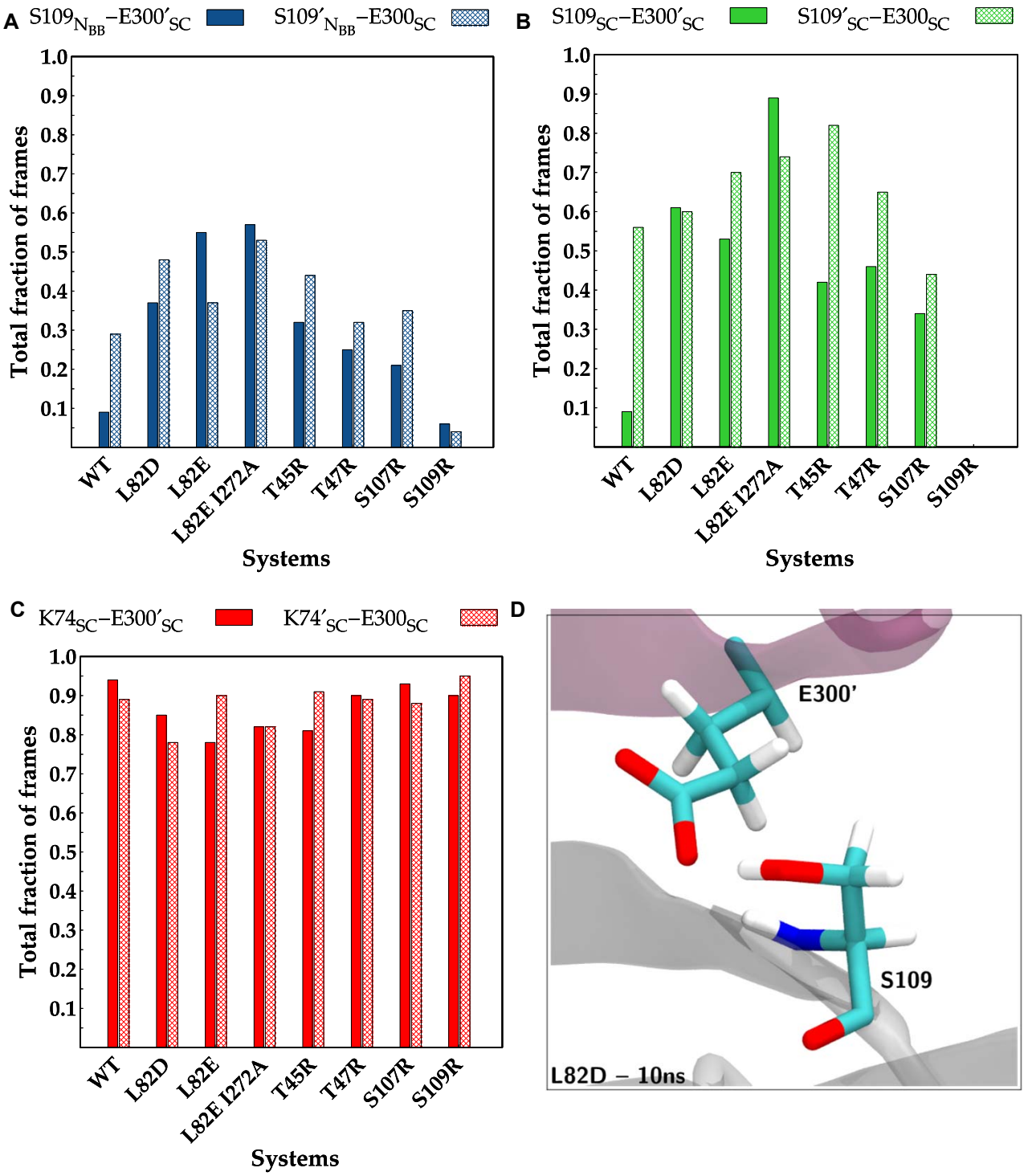

Figure S19. Total fraction of the frames that a hydrogen bond exists between (A) the backbone nitrogen atom of S109 and the sidechain of E300' (solid), and the backbone nitrogen atom of S109' and the sidechain of E300 (pattern fill); (B) the sidechains of S109 and E300' (solid), and sidechains of S109' and E300 (pattern fill); (C) the sidechains of K74 and E300' (solid), and sidechains of K74' and E300 (pattern fill). (D) The three-dimensional representation of the depicted interaction obtained from the trajectory of L82D variant at 10 ns. Sidechain is depicted with subscript "SC" while the backbone Nitrogen atoms are depicted with subscript "N_{BB}."

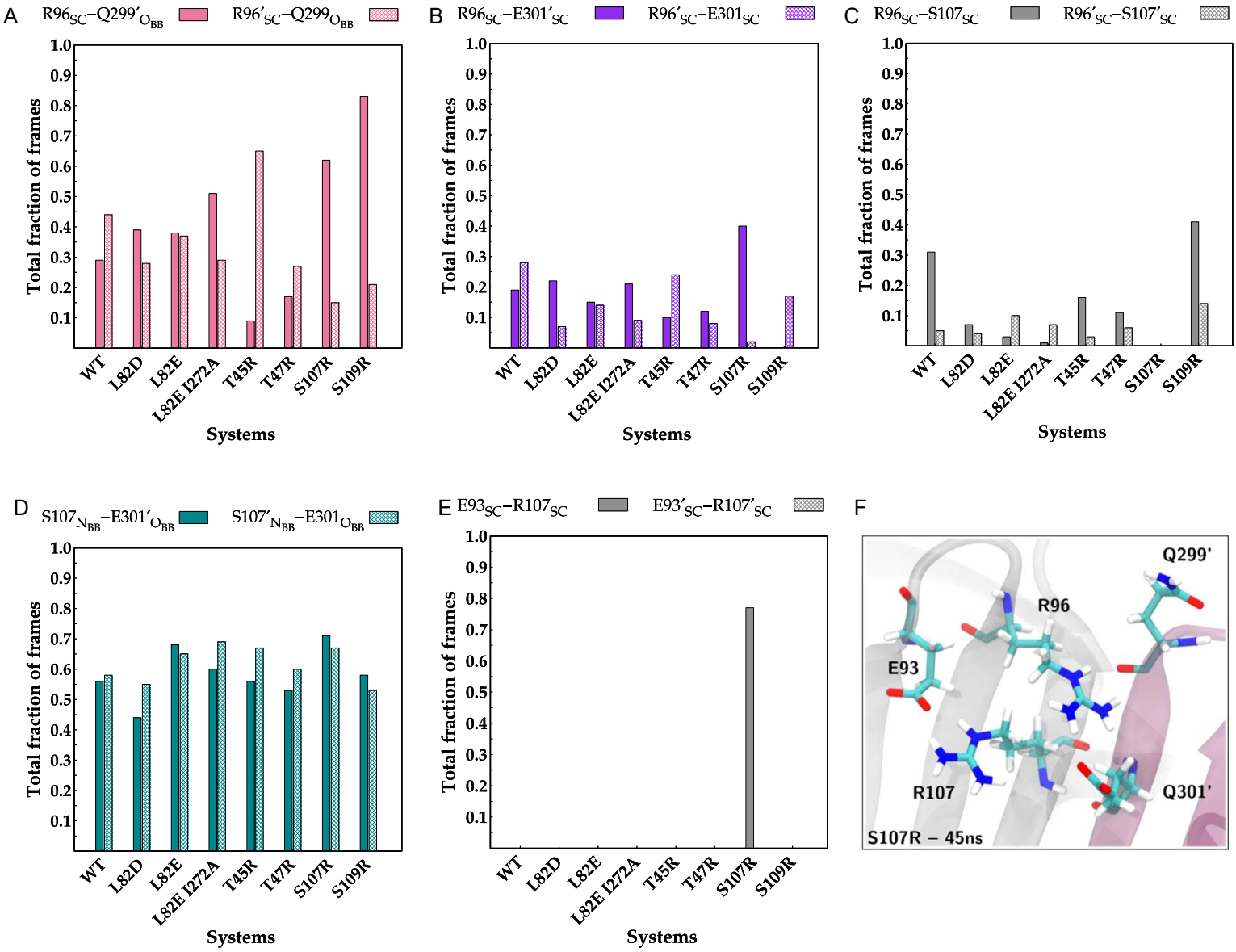

Figure S20. Total fraction of the frames that a hydrogen bond exists between (A) the sidechain of R96 and the backbone oxygen atom of Q299' (solid), and the sidechain of R96' and the backbone oxygen atom of Q299 (pattern fill); (B) the sidechains of R96 and E301' (solid), and the sidechains of R96' and E301 (pattern fill); (C) the sidechains of R96 and S107 (solid), and the sidechains of R96' and S107' (pattern fill); (D) the backbone nitrogen atom of S107 and the backbone oxygen atom of E301' (solid), and the backbone nitrogen atom of S107' and the backbone oxygen atom of E301 (pattern fill); (E) the sidechains of E93 and R107 (solid), and the sidechains of E93' and R107' (pattern fill). (F) The three-dimensional representation of the depicted interaction obtained from the trajectory of S107R variant at 45 ns. Sidechains are depicted with subscript "SC" while Nitrogen and Oxygen atoms on the backbone are depicted with subscripts "N_{BB}" and "O_{BB}," respectively.

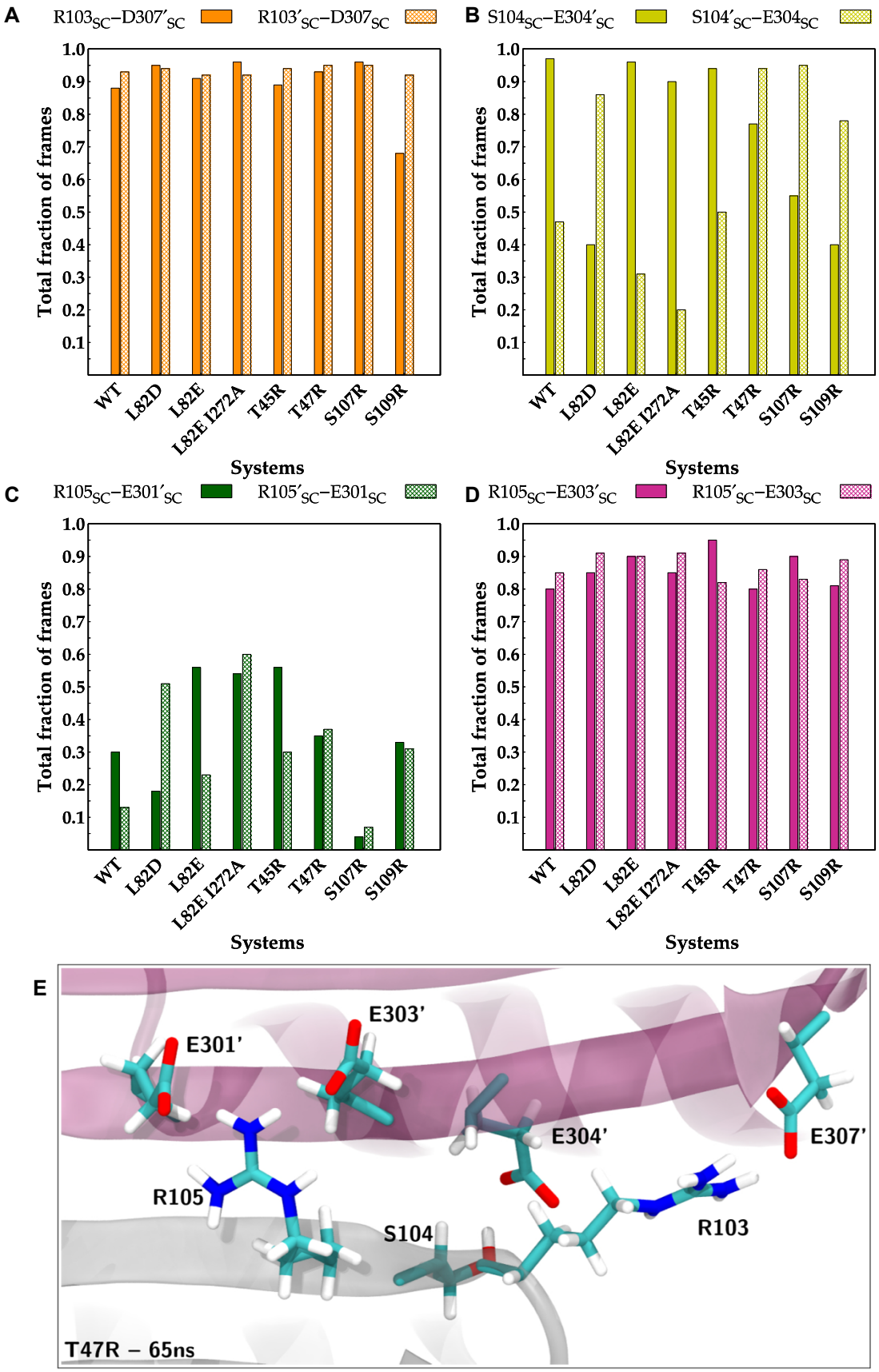

Figure S21. Total fraction of the frames that a hydrogen bond exists between (A) the sidechains of R103 and D307' (solid), and the sidechains of R103' and D307 (pattern fill); (B) the sidechains of S104 and E304' (solid), and the sidechains of S104' and E304 (pattern fill); (C) the sidechains of R105 and E301' (solid), and the sidechains of R105' and E301 (pattern fill). (D) the sidechains of R105 and E303' (solid), and the sidechains of R105' and E303 (pattern fill). (E) The three-dimensional representation of the depicted interactions obtained from the trajectory of T47R variant at 65 ns. Sidechains are depicted with subscript "SC."